Deciphering the Mechanism of O_2 Reduction with Electronically Tunable Non-Heme Iron Enzyme Model Complexes

Roshaan Surendhran,[†] Alexander A. D'Arpino,[†] Bao Y. Sciscent,[†] Anthony F. Cannella,[†] Alan E. Friedman,[†] Samantha N. MacMillan,[§] Rupal Gupta,[‡] David C. Lacy*[†]

[†] Department of Chemistry, University at Buffalo, State University of New York, Buffalo, NY 14260, United States

[‡] Department of Chemistry, College of Staten Island, City University of New York, Staten Island, NY 10314, United States

§ Department of Chemistry and Chemical Biology, Cornell University, Ithaca, NY 14853, United States

*Corresponding Author
E-mail: DCLacy@buffalo.edu

Contents **Page**

Methods	S2
Synthesis and NMR Spectra of Ligands	S2 - 14
Figure S1. ^{1}H-NMR N*H* ligand resonance vs. Hammett sigma parameter	S14
Synthesis and NMR spectra (Figure 2a-h) of Fe(II) and Zn(II) complexes	S15 - 22
Table S1. Comparative crystallographic metrics	S23
Figure S3. Crystal structures	S23
Figure S4. Mössbauer Spectrum of Fe	S23
Synthesis of **2a** and **2b**	S24 - S25
Figure S5. UV-vis and ^{1}H-NMR spectra of **2a** and **2b**	S24 - S25
Figure S6. Uv-vis spectra comparison of **2b** and **2** generated at low concentration	S26
Figure S7. Additional linear free energy relationship plots	S27
Derivation of rate law and representative plots and figures	S28 - 29
Figure S8. Representative plots for order determination of iron	S30
Table S2. Values of k_{obs}	S30
Figure S9. Order of $[O_2]$ determination	S31
Figure S10. Plot of $1/k_{obs}$ vs. $1/[O]_2$ for $\mathbf{1^H}$	S31
Figure S11. First plots for the reaction of O_2 with $\mathbf{1^{Cl}}$ and $\mathbf{1^{NO2}}$	S31
Table S3. Data for Eyring plot	S33
Kinetic Methods and Mass transport analysis	S34 - 40
References	S41

Physical Methods
NMR experiments were performed on Varian Mercury-300 MHz, Inova-400 MHz and Inova-500 MHz spectrometers. GCMS analysis of reaction mixtures was performed using an HP 5890 Series II GC coupled with a HP 5972 Series Mass Selective Detector. Transmission and ATR-FTIR spectra were collected inside of a VAC Atmospheres Omni glovebox using a Bruker Alpha IR spectrometer with ALPHA-P Platinum ATR module (diamond crystal). UV-vis spectra were collected using a 8154 Agilent spectrophotometer equipped with an Unisku cryostat. CHN combustion analyses were performed by Robertson Microlit Laboratories, NJ USA. Fourier Transform Matrix Assisted Laser Desorption/Ionization (FT MALDI) mass spectra (MS) were collected using a Bruker Daltonics SolariX 12 tesla Fourier Transform Ion Cyclotron Resonance Mass Spectrometer equipped with a dual source and anthracene as the matrix compound. Matrix-Free LDIMS was used for the metal complexes. Mössbauer spectra were collected at Carnegie Mellon University using a Janis Research variable temperature dewar. Isomer shifts are reported relative to Fe metal at 298 K.

Crystallographic methods
Low-temperature X-ray diffraction data for **2a**, **2b**, $[Me_4N]_2[Fe\mathbf{L}^{H}(OAc)]$ (Fe-H), and $[Me_4N]_2[Zn\mathbf{L}^{H}(OAc)]$ (Zn-H) were collected at Cornell University on a Rigaku XtaLAB Synergy diffractometer coupled to a Rigaku Hypix detector with either Mo Kα radiation (λ = 0.71073 Å) or Cu Kα radiation (λ = 1.54184 Å), from a PhotonJet micro-focus X-ray source at 100 K. The diffraction images were processed and scaled using the CrysAlisPro software.[1] Low-temperature X-ray diffraction data for $[Me_4N]_2[Fe\mathbf{L}^{NO2}(OAc)]$ (Fe-NO_2) and $[Me_4N]_2[Zn\mathbf{L}^{NO2}(OAc)]$ (Zn-NO_2) were collected at University at Buffalo on a Bruker SMART APEX2 CCD diffractometer installed at a rotating anode source (Mo$K\alpha$ radiation, α=0.71073 Å) at 90 K. The diffraction images were processed and scaled using the APEX2 software.[2] The structures were solved either through intrinsic phasing using SHELXT[3] or by direct methods using SHELXS[4] and refined against F^2 on all data by full-matrix least squares with SHELXL[5] following established refinement strategies.[6] All non-hydrogen atoms were refined anisotropically. All hydrogen atoms bound to carbon were included in the model at geometrically calculated positions and refined using a riding model. The isotropic displacement parameters of all hydrogen atoms were fixed to 1.2 times the Ueq value of the atoms they are linked to (1.5 times for methyl groups). The unit cells of **2b**, and $[Me_4N]_2[Fe\mathbf{L}^{NO2}(OAc)]$ (Fe-NO_2) contain disordered solvent molecules that could not be satisfactorily modeled; these were consistent with solvent molecules (e.g., water, ether) and have been treated as diffuse contributions to the overall scattering without specific atom positions using the solvent mask routine in Olex2.[7]

Synthetic Methods
All reagents were obtained from commercial vendors and used as received unless otherwise noted. The ligands were synthesized according to a modified procedure[1] using standard Schlenk line techniques. The procedure outlined for $\mathbf{H_3L^H}$ was followed for all of the ligands with exceptions noted below. All metal complexes were synthesized in nitrogen filled Genesis VAC Atmosphere glovebox and handled under inert atmosphere. Solvents used for metal complex synthesis and kinetics were obtained off a PPT solvent purification system and subsequently stored over activated 3 Å sieves. Potassium hydride (obtained as a 30% dispersion in mineral oil) was purified from the oil by washing with petroleum ether (5 x 10 mL), diethyl ether (once with 10 mL), and then petroleum ether (3 x 10 mL) and vacuum dried in a glass-fritted funnel.

Synthesis of $\mathbf{H_3L^R}$ ligands: General ligand synthesis strategy (R = H, F, Cl, Br, CF_3, CN, NO_2, NMe_2, OMe, Me, Et)

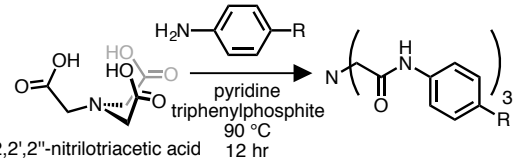

2,2',2''-nitrilotris(N-phenylacetamide) ($\mathbf{H_3L^H}$): 17.5 ml of pyridine was degassed by sparging with argon for 30 minutes in a three neck round bottom flask followed by addition of nitrilotriacetic acid (NTA, 3.25

g, 17 mmol) and a positive pressure of argon was maintained throughout the synthesis. To the NTA slurry, aniline (4.8 ml, 52.7 mmol) was added dropwise with a pipet and stirred for 1 hour. The mixture was then heated to 80 °C and triphenylphosphite (18.2 ml, 69.5 mmol) was slowly added using a drop funnel. The reaction was refluxed at 90 °C overnight under argon. The reaction was cooled to room temperature and 50 ml of diethyl ether is added and stirred for 1 h. A white solid precipitated and was filtered open to air and washed three times with 10 ml of chloroform and twice with 10 ml of diethyl ether to yield 6.3 g of a white powder (89%) of $\mathbf{H_3L^H}$. This material was further dried under vacuum at 100° C overnight before being brought into a glovebox. ^{1}H NMR (DMSO-d_6, 300 MHz) δ 3.65 (s, 6H, –CH_2–), δ 7.04 (t, 3H, p-C_6H_6), δ 7.31 (t, 6H, m-C_6H_6), δ 7.65 (d, 6H, o-C_6H_6), δ 10.30 (s, 3H, –NH). ^{13}C NMR (DMSO-d_6) δ 58.94, δ 119.52, δ 123.78, 129.23, δ 139.25, δ 170.49. ATR-FTIR (cm^{-1}): 3310, 3268, 3238, 3136, 3059, 3044, 2933, 2902, 2842, 1689, 1651, 1619, 1597, 1539. HRMS (MALDI/FT-ICR) m/z: [M - H]$^-$ Calcd for $C_{24}H_{23}N_4O_3$ 415.1776; Found 415.1786.

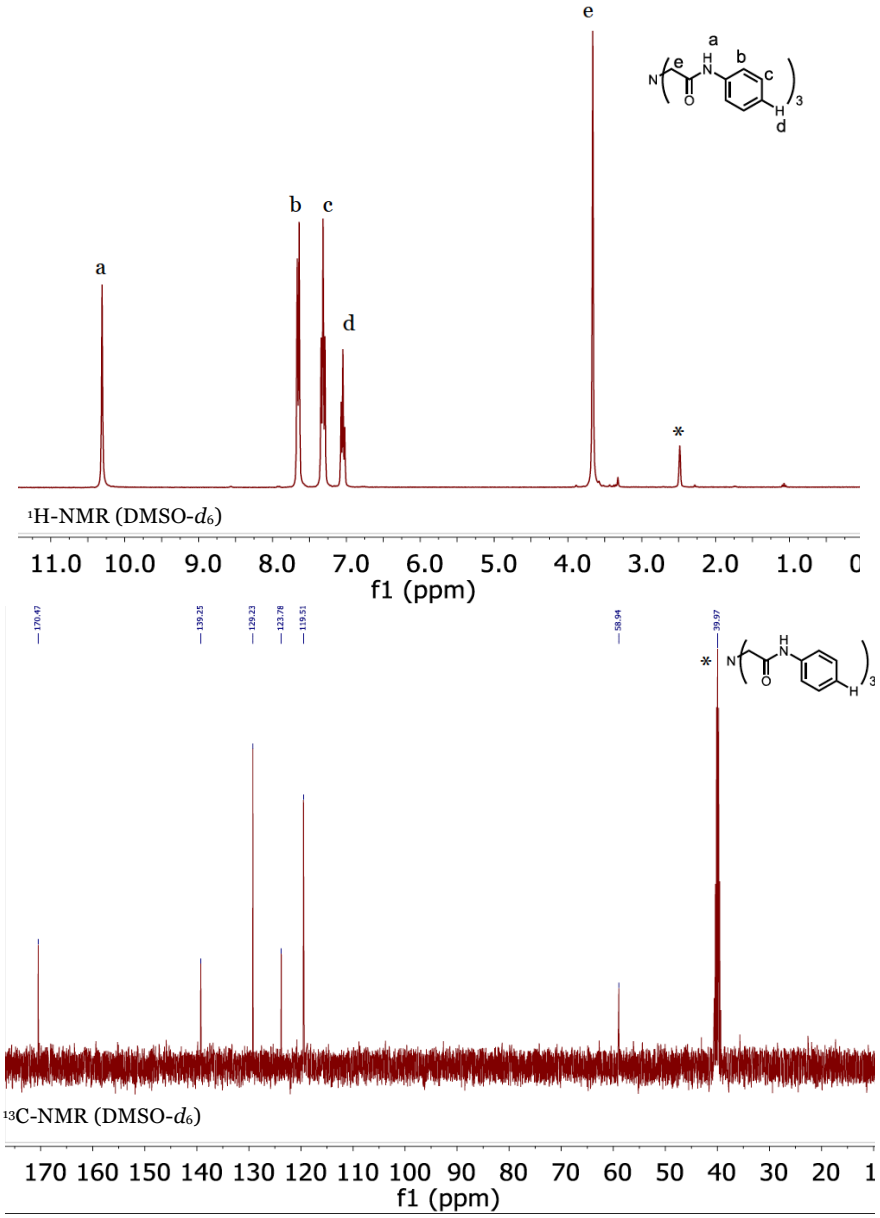

*2,2',2''-nitrilotris(N-(4-fluorophenyl)acetamide) (**H_3L^F**)*: p-fluoroaniline (5.00 mL, 52.8 mmol), NTA (3.31 g, 17.3 mmol) pyridine (13.3 mL), triphenylphosphite (14.0 mL, 53.4 mmol). White powder 5.9 g (73% based on NTA). ^{1}H NMR (DMSO-d_6, 300 MHz) δ 10.34 (3 H, s, N*H*), 7.65 (6 H, dd, Ar*H*), 7.15 (6 H, dd, Ar*H*), 3.64 (6 H, s, CH_2). ^{13}C NMR (DMSO-d_6, 400 MHz) δ 170.32, 135.65, 121.27, 121.20, 115.89, 115.67, 58.81. ^{19}F NMR (DMSO-d_6, 300 MHz) δ -119.3 (multiplet). ATR-FTIR: (cm^{-1}) 3306, 3278, 3224, 3156, 3067, 2901, 1691, 1658, 1644, 1620, 1562, 1533, 1505. HRMS (MALDI/FT-ICR) m/z: [M - H]$^-$ Calcd for $C_{24}H_{20}F_3N_4O_3$ 469.1493; Found 469.1508.

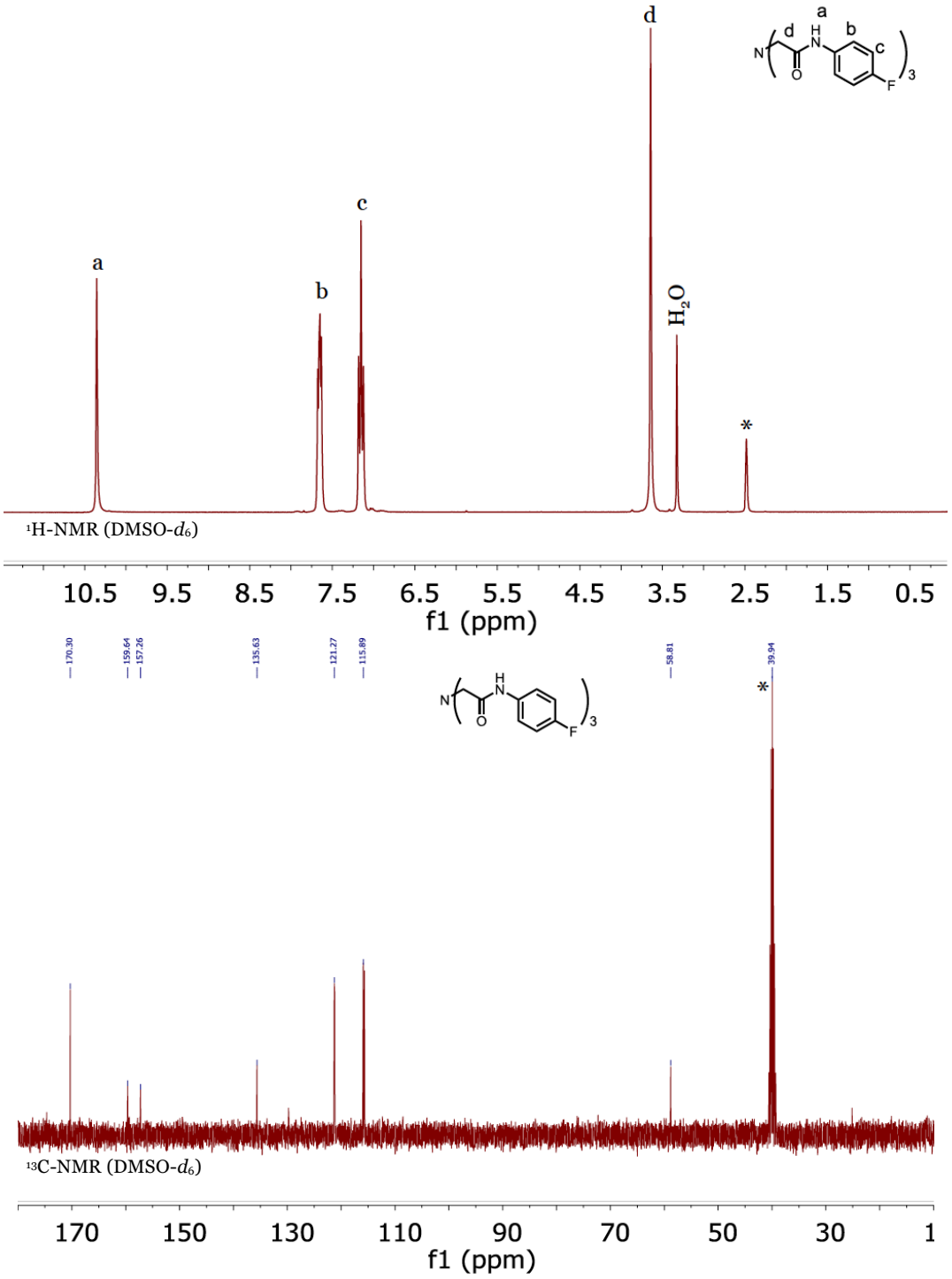

*2,2',2''-nitrilotris(N-(4-chlorophenyl)acetamide) (**H_3L^{Cl}**)*: p-chloroaniline (6.74 g, 52.8 mmol), NTA (3.29 g, 17.2 mmol), pyridine (13.3 mL), triphenylphosphite (13.7 mL, 52.3 mmol). White powder 6.6 g (73% based on NTA). ^{1}H NMR (DMSO-d_6, 300 MHz) δ 10.40 (3 H, s, N*H*), 7.66 (6 H, d, Ar*H*), 7.36 (6 H, d, C*H*), 3.65 (6 H, s, CH_2). ^{13}C NMR (DMSO-d_6, 400 MHz) 170.62, 138.15, 129.15, 127.34, 121.06, 58.87. ATR-FTIR: (cm^{-1}) 3317, 3183, 3038, 2911, 1689, 1659, 1608, 1595, 1535. HRMS (MALDI/FT-ICR) m/z: [M - H]$^-$ Calcd for $C_{24}H_{20}Cl_3N_4O_3$ 517.06065; Found 517.06266.

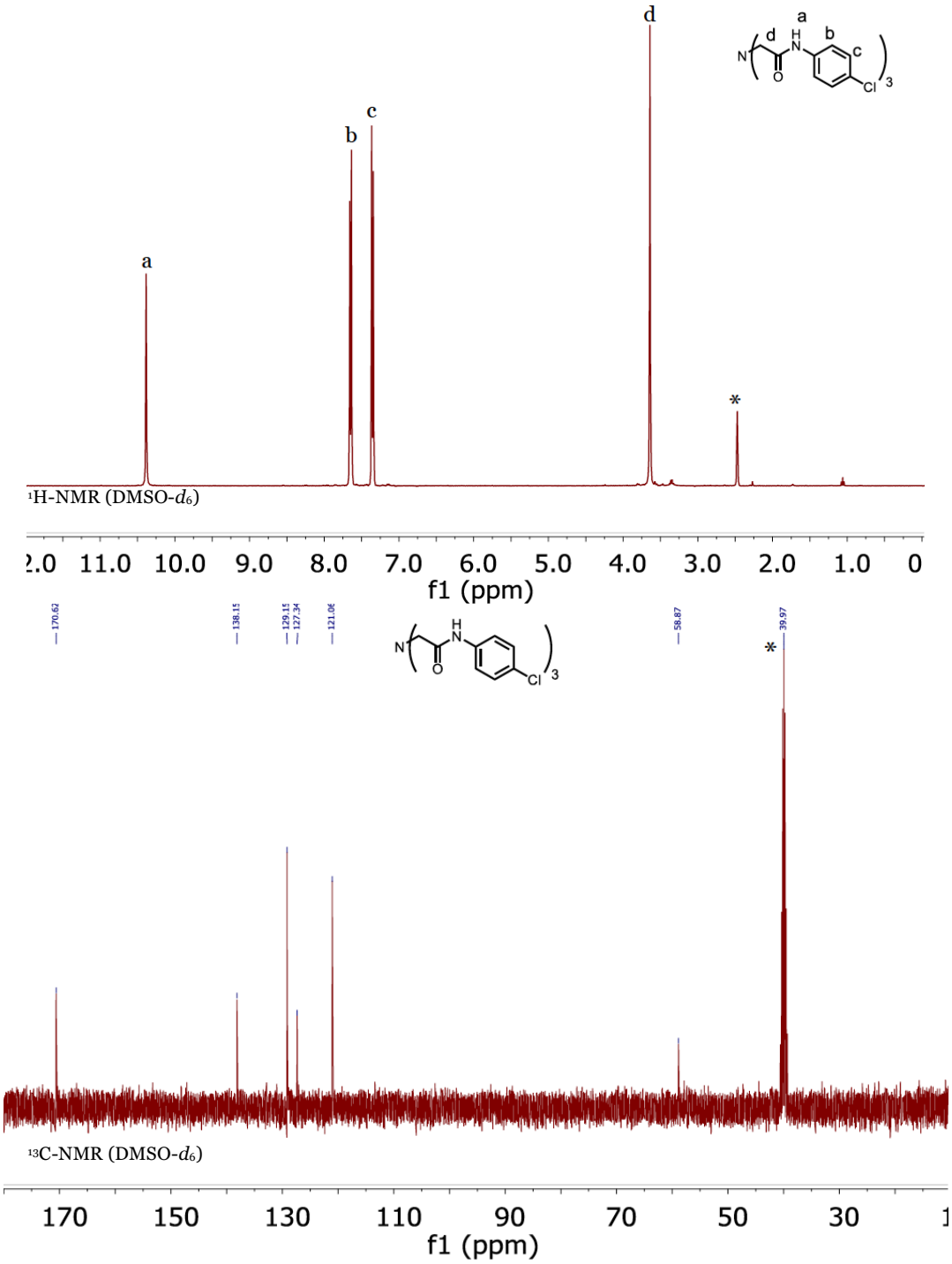

*2,2',2''-nitrilotris(N-(4-bromophenyl)acetamide) (**H_3L^{Br}**)*: NTA (3.3 g, 17.4 mmol), pyridine (10 mL), 4-bromoaniline (9.0 g, 52.3 mmol), triphenylphosphite (52.6 mmol, 13.8 mL). Dried overnight under vacuum at 55 °C. White powder 9.7 g (85% based on NTA). ^{1}H-NMR (DMSO-d_6, 300 MHz, 298 K): δ 10.39 (3H, s, 3N*H*), δ 7.59 (6H, d, *CH*), 7.50 (6H, d, *CH*), 3.71 (6H, s, *CH*). ^{13}C NMR (DMSO-d_6, 400 MHz) 170.66, 138.57, 132.06, 121.44, 115.37, 58.90. ATR-FTIR: (cm^{-1}) 3324, 3287, 3254, 3221, 3136, 3084, 2901, 2860, 1679, 1665, 1606, 1589, 1542, 1525. HRMS (MALDI/FT-ICR) m/z: [M - H]$^-$ Calcd for $C_{24}H_{20}Br_3N_4O_3$ 648.90910; Found 648.91318.

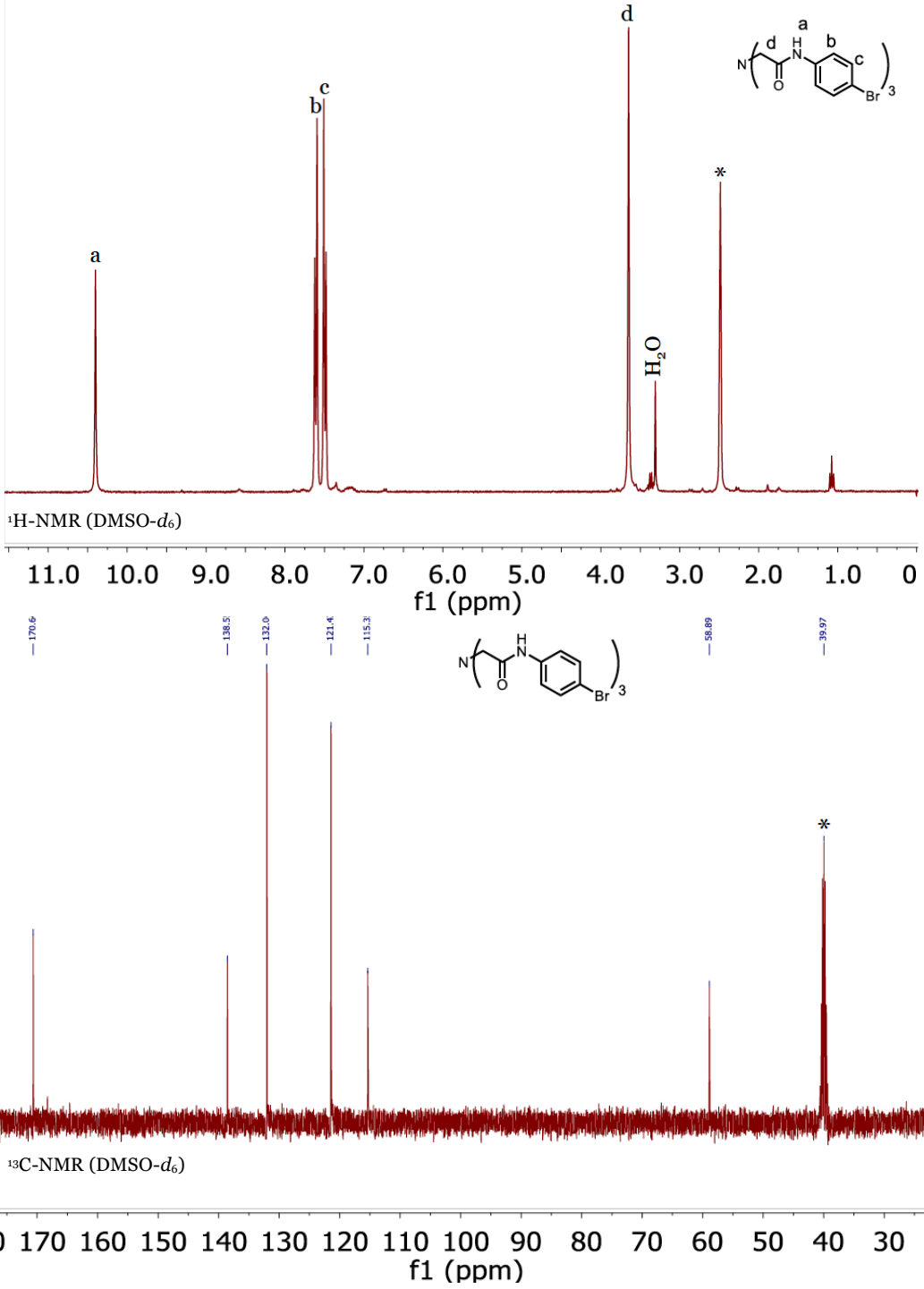

*2,2',2''-nitrilotris(N-(4-(trifluoromethyl)phenyl)acetamide) (**$H_3L^{CF_3}$**)*: p-trifluoromethyl aniline (2.45 g, 1.9 ml, 15 mmol), NTA (0.95 g, 5.0 mmol), pyridine (4 mL), triphenylphosphite (4 mL, 15 mmol). The final mixture was stirred for 19 hours at 90 °C. After 19 hours, the flask was allowed to cool to room temperature and solvent removed *in vacuo*. The resulting oily mixture was cooled in a freezer for several hours. Isopropanol, chilled to dry ice temperature, was added to the crude material causing a white precipitate to form. The solids were filtered cold using a pre-chilled frit and washed with dry ice chilled isopropanol. The solids were further dried with vacuum to yield a white product (0.62 g, 20% based on NTA). ^{1}H NMR (DMSO-d_6, 300 MHz): δ 3.72 (s, 6H, –CH_2–), 7.68 (d, 6H, m-C_6H_6, J = 9 Hz), 7.84 (d, 6H, o-C_6H_6, J = 6 Hz), δ 10.62 (s, 3H, –*NH*). ^{13}C NMR (DMSO-d_6, 300 MHz): δ 171.19, 142.72, 126.58, 123.80 (q, J = 126, 255), 122.99, 119.42, 59.03. ^{19}F NMR (DMSO-d_6, 376 MHz): δ -60.38. ATR-FTIR: (cm^{-1}) 3293, 1697, 1679, 1617, 1603, 1528, 1507. HRMS (MALDI/FT-ICR) m/z: [M - H]$^-$ Calcd for $C_{27}H_{20}F_9N_4O_3$ 619.1397; Found 619.1407.

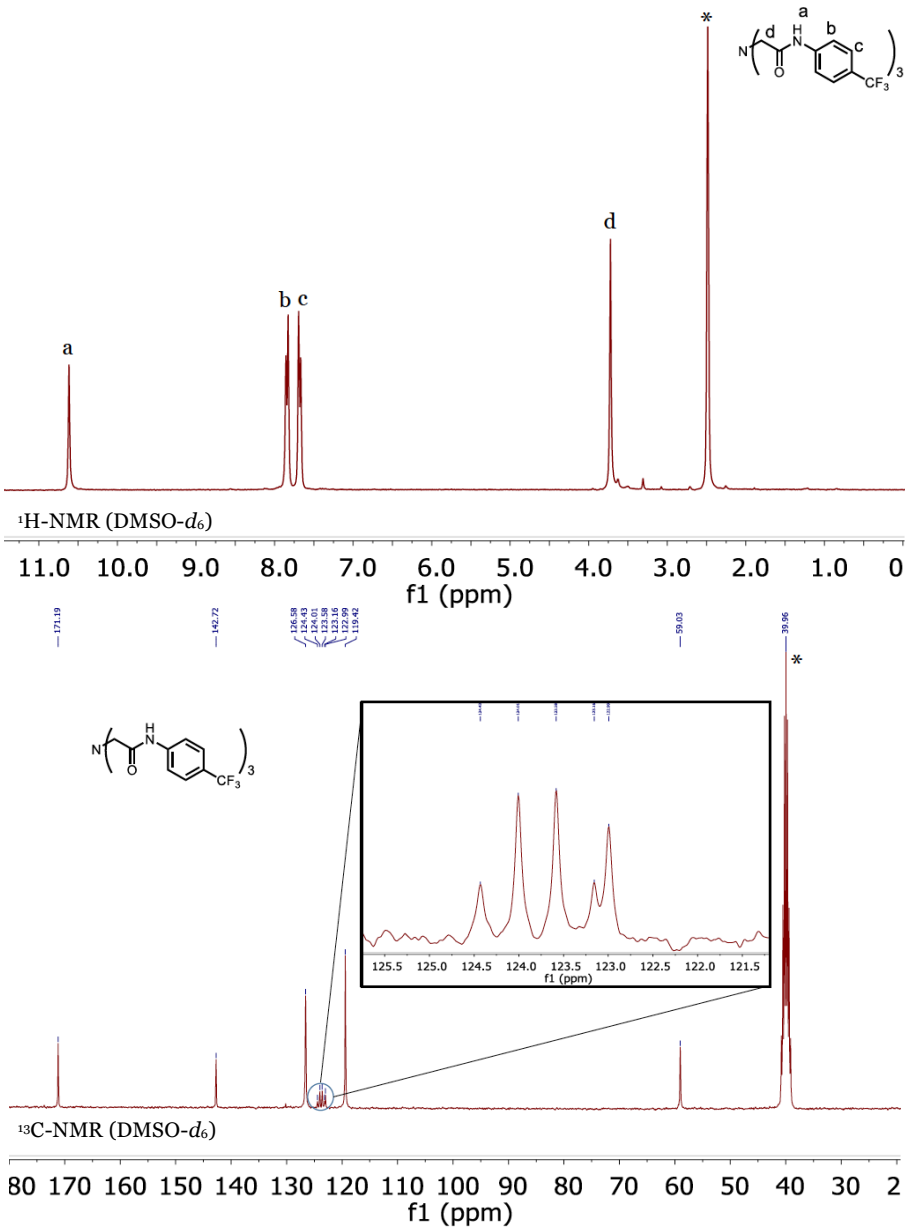

*2,2',2''-nitrilotris(N-(4-cyanophenyl)acetamide) (**H_3L^{CN}**)*: 4-aminobenzonitrile (3.1 g, 26.2 mmol), NTA (1.0 g, 5.3 mmol), pyridine (4 mL), triphenylphosphite (4.1 mL, 15.7 mmol). The final mixture was stirred for 92 hours. The flask was allowed to cool to room temperature and diethyl ether (15 mL) was added and stirred for 90 minutes, giving a light brown solid 1.90 g (73% based on NTA). Alternatively, the reaction was stirred for a shorter period (42 hours) with a reduced yield (50.3%). ^{1}H NMR (DMSO-d_6, 400 MHz) δ 10.63 (3 H, s, N*H*), 7.76 (12 H, s, Ar*H*), 3.68 (6 H, s, CH_2). ^{13}C NMR (DMSO-d_6, 400 MHz) δ 171.40, 143.29, 133.80, 119.58, 119.46, 105.58, 59.02. ATR-FTIR: (cm^{-1}) 3320, 3288, 3163, 3092, 3043, 2925, 2227, 2217, 1705, 1668, 1595, 1526. HRMS (MALDI/FT-ICR) m/z: [M - H]$^-$ Calcd for $C_{27}H_{20}N_7O_3$ 490.16331; Found 490.16443.

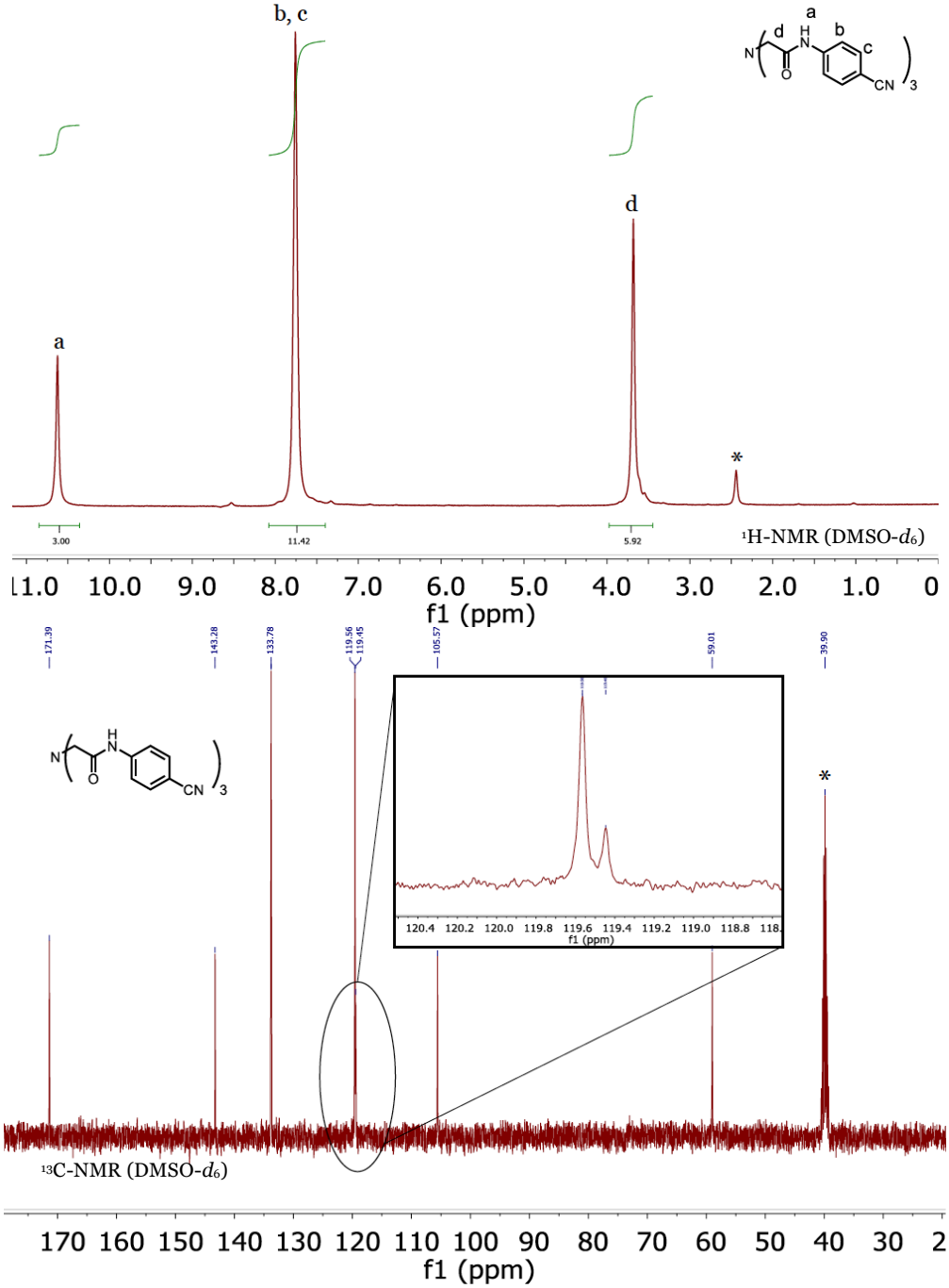

2,2',2''-nitrilotris(N-(4-(dimethylamino)phenyl)acetamide) (***H*$_3$*L*^{NMe2}***): 4-(dimethylamino)aniline (3.04 g, 22.3 mmol), NTA (1.00 g, 5.23 mmol), pyridine (4 mL), triphenylphosphite (4.2 mL, 16.0 mmol). The final mixture was stirred for 23 hours at 90 °C. Off-white solid 2.0 g (70% based on NTA). ^{1}H-NMR (DMSO-d_6, 300 MHz, 298 K): δ 10.05 (3H, s, N*H*), δ 7.44 (6H, d, C*H*), δ 6.70 (6H, d, C*H*), δ 3.57 (6H, s, C*H*), δ 2.87 (20H, s, C*H*). ATR-FTIR: (cm^{-1}) 3235, 1436, 1169, 1154, 1118, 1092, 1068, 1029, 996, 764, 750, 720, 692, 535, 506, 463,442. ^{13}C NMR (DMSO-d_6, 400 MHz) δ 169.46, 147.60, 128.99, 121.04, 113.09, 59.02, 40.90. ATR-FTIR: (cm^{-1}): 2801, 1594, 1515. HRMS (MALDI/FT-ICR) m/z: [M - H]$^-$ Calcd for $C_{30}H_{38}N_7O_3$ 544.30416; Found 544.30727.

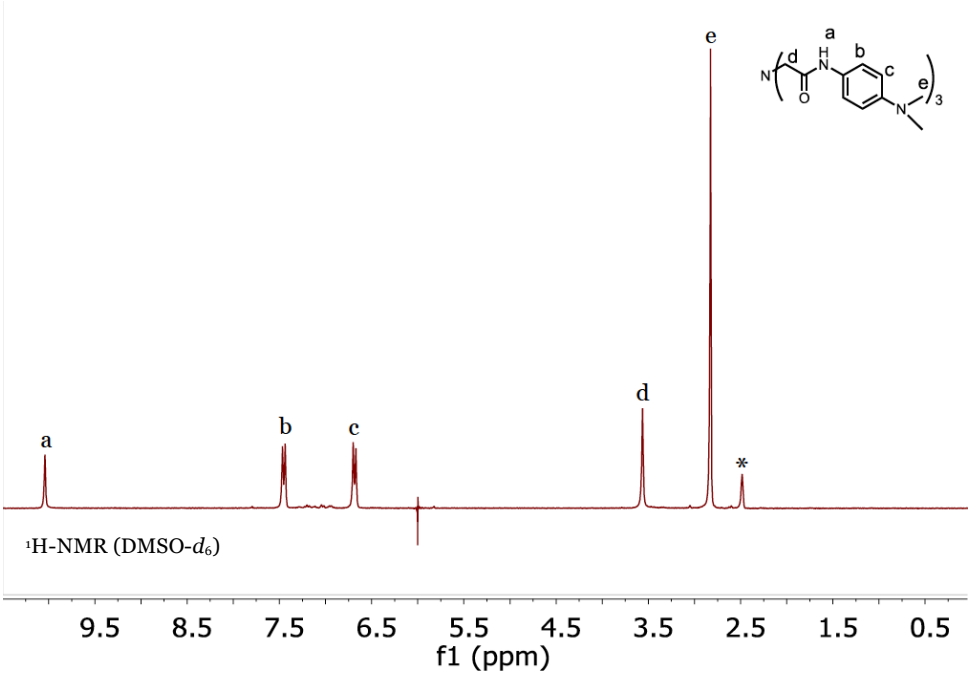

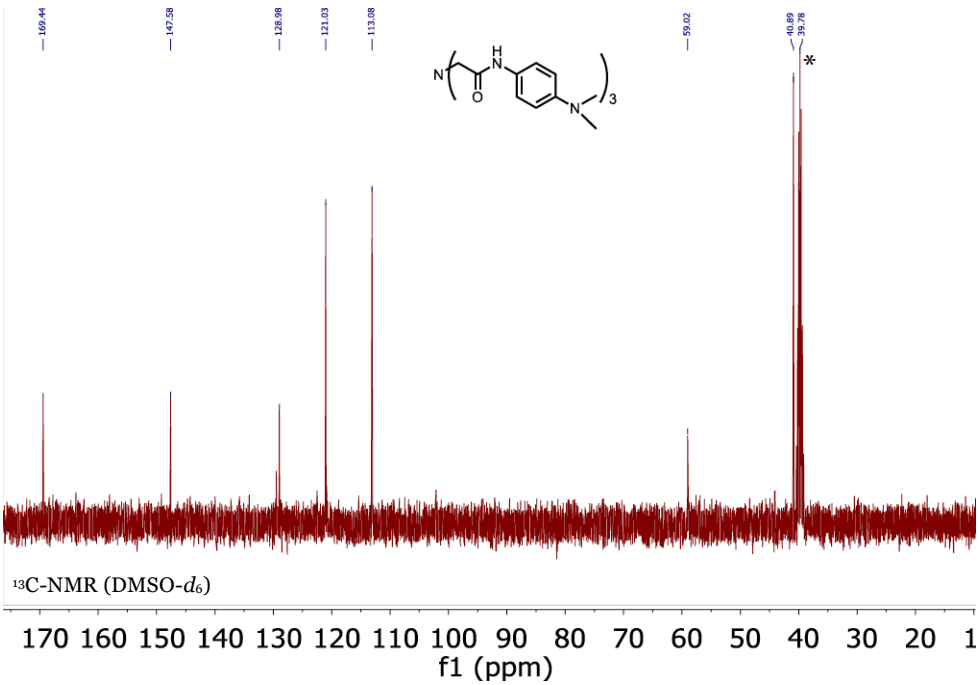

*2,2',2''-nitrilotris(N-(4-methoxyphenyl)acetamide) (**H_3L^{OMe}**)*: *p*-anisidine (6.45 g, 52.4 mmol), NTA (3.3 g, 17.3 mmol), pyridine (13.3 mL), triphenylphosphite (14.0 mL, 53.4 mmol). Final mixture stirred for 12 hours at 90 °C. White powder 6.66 g (76% based on NTA). ^{1}H NMR (DMSO-d_6, 300 MHz) δ 10.18 (3 H, s, N*H*), 7.55 (6 H, d, C*H*), 6.89 (6 H, d, C*H*), 3.71 (9 H, s, CH_3), 3.60 (6 H, s, CH_2). ^{13}C NMR (DMSO-d_6, 400 MHz) δ 169.84, 155.68, 132.42, 121.01, 114.33, 58.87, 55.57. ATR-FTIR: (cm^{-1}) 3179, 3127, 2996, 2837, 1672, 1646, 1615, 1601, 1540, 1507. HRMS (MALDI/FT-ICR) m/z: [M - H]$^-$ Calcd for $C_{27}H_{29}N_4O_6$ 505.20926; Found 505.21040.

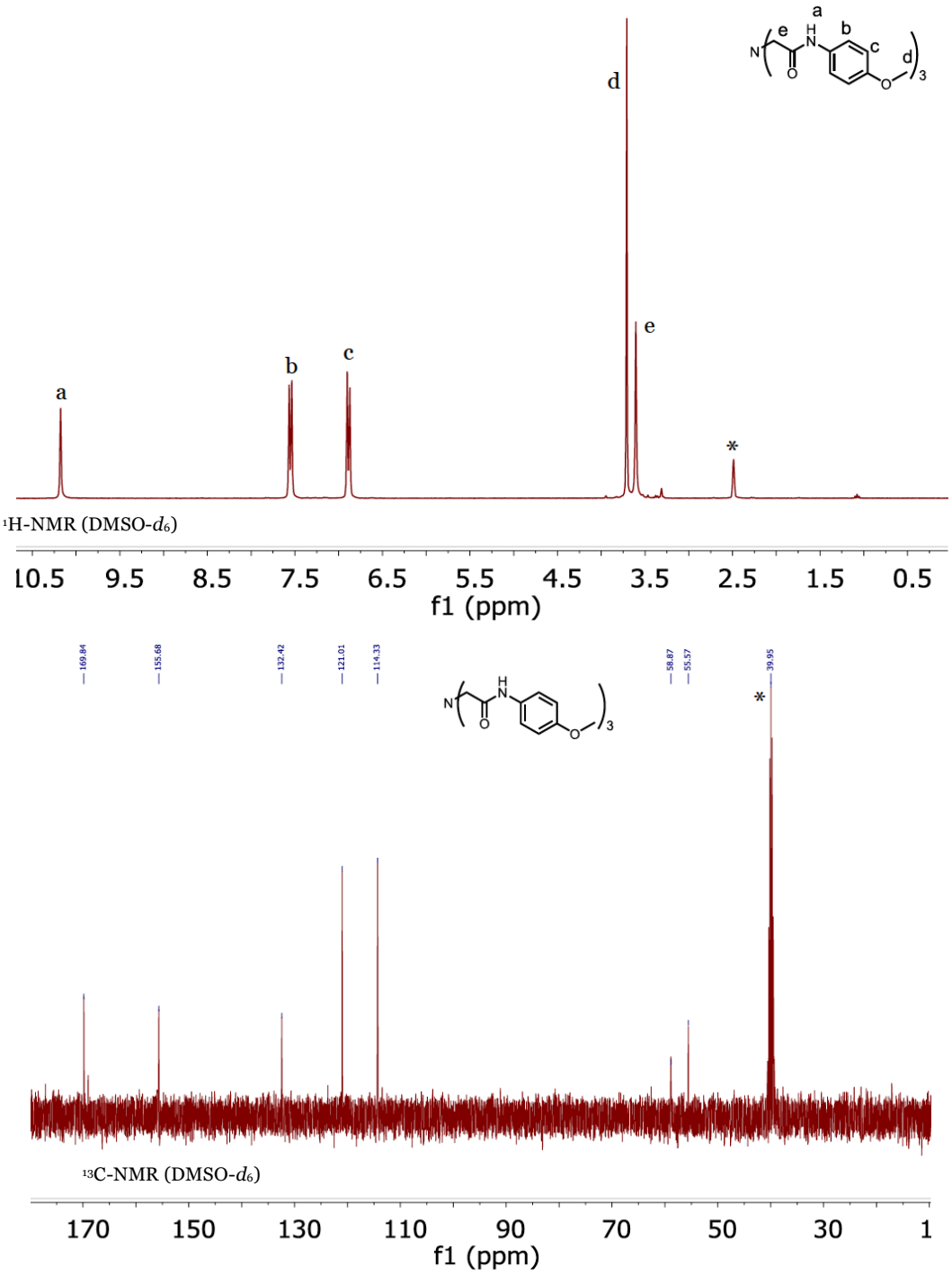

2,2',2''-nitrilotris(N-(p-tolyl)acetamide) (***H_3L^{Me}***): p-toluidine (6.77 g, 63.2 mmol), NTA (3.32 g, 17.4 mmol), pyridine (13.3 mL), triphenylphosphite (14.0 mL, 53.2 mmol). Final mixture stirred for 18 hours at 90 °C. White powder 6.46 g (81% based on NTA). ^{1}H-NMR (DMSO-d_6, 300 MHz, 298 K): δ 10.24 (3H, s, N*H*), 7.54 (6H, d, J = 8.4 Hz, C*H*), 7.13 (6H, d, J = 8.4 Hz, C*H*), 3.63 (6H, s, C*H*), 2.25 (9H, s, *CH*). ^{13}C NMR (DMSO-d_6, 300 MHz) δ 170.21, 136.79, 132.67, 129.61, 119.52, 58.93, 20.91. ATR-FTIR (cm^{-1}): 3309, 3208, 3177, 3120, 3028, 2922, 2893, 1675, 1648, 1605, 1593, 1535, 1511. HRMS (MALDI/FT-ICR) m/z: [M - H]$^-$ Calcd for $C_{27}H_{29}N_4O_3$ 457.2245; Found 457.2258.

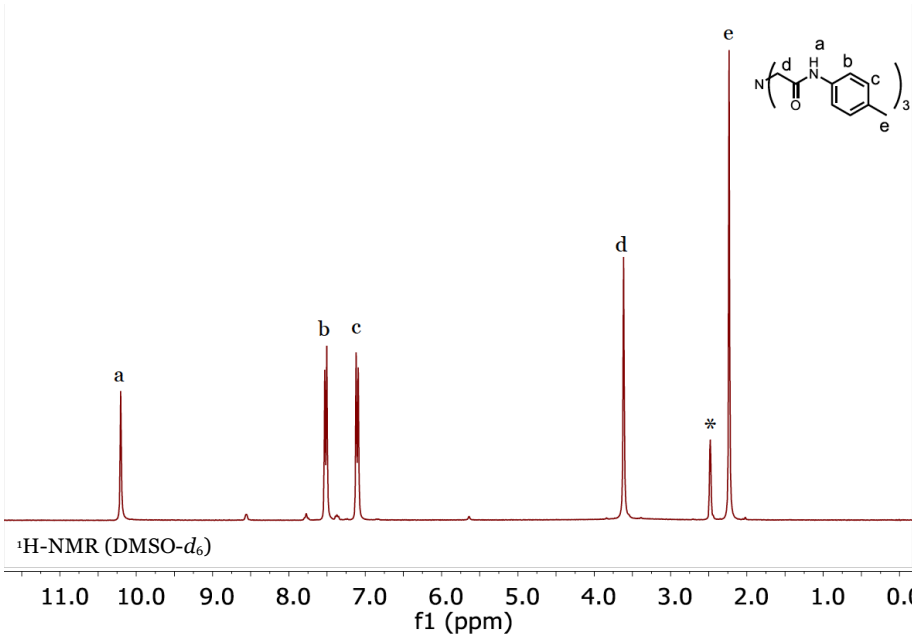

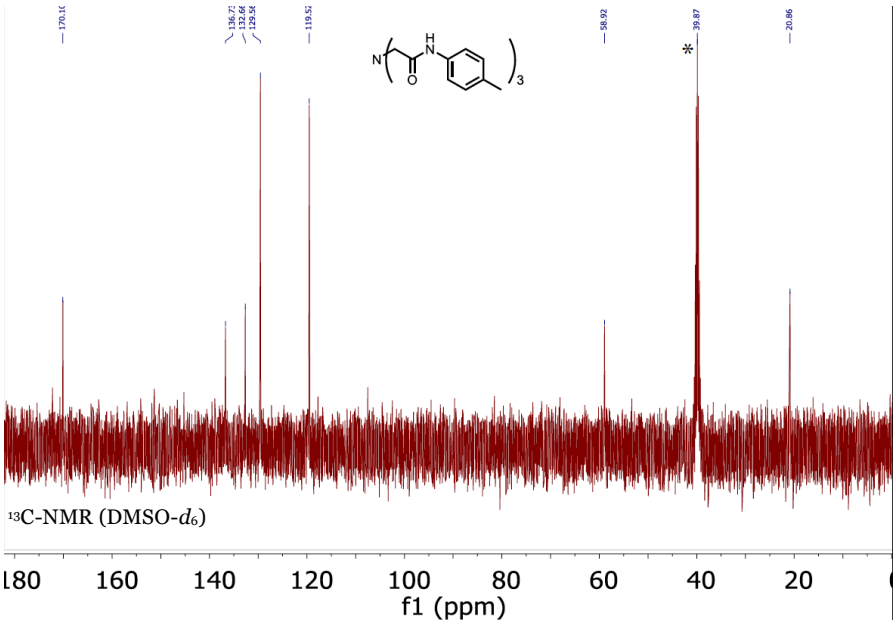

2,2',2''-nitrilotris(N-(4-ethylphenyl)acetamide) (***H*$_3$*L*^{Et}**): 4-ethylaniline (41.3 mmol, 5.0 g), NTA (2.63 g, 13.7 mmol), pyridine (10 mL), triphenylphosphite (10.9 mL, 41.6 mmol). The reaction mixture was cooled to room temperature and filtered directly glass-fritted funnel with suction and washed copious amounts of chloroform followed by diethyl ether. The solids were further dried under vacuum at 50 °C overnight and brought into a glovebox. White powder 4.8 grams (70% based on NTA). ^{1}H-NMR (DMSO-d^6, 400 MHz, 298 K): δ 10.18 (3H, s, 3N*H*), δ 7.49 (6H, d, *J* = 8.0 Hz, *CH*), 7.09 (6H, d, *J* = 8.4 Hz, *CH*), 3.57 (6H, s, *CH*), 2.48 (6H, q, *J* = 15.2 Hz, *CH*), 1.095 (9H, q, *J* = 1.6 Hz, *CH*). ^{13}C NMR (DMSO-d$_6$, 400 MHz): δ 170.15, 139.13, 136.95, 128.38, 119.59, 58.93, 28.04, 16.13. ATR-FTIR: (cm^{-1}) 3235, 1436, 1169, 1154, 1118, 1092, 1068, 1029, 996, 764, 750, 720, 692, 535, 506, 463,442. HRMS (MALDI/FT-ICR) m/z: [M - H]$^-$ Calcd for $C_{30}H_{35}N_4O_3$ 499.27146; Found 499.27466.

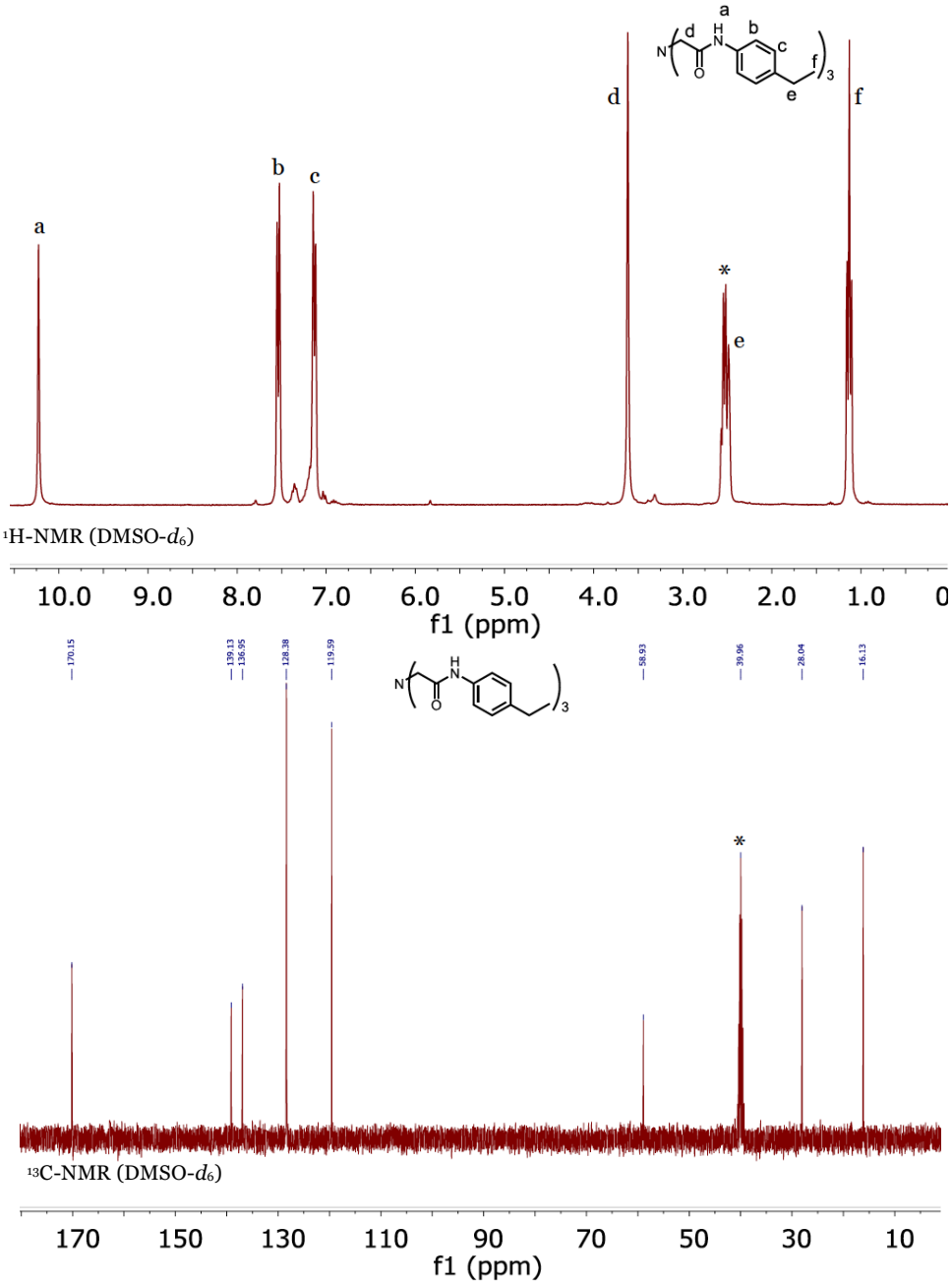

2,2',2''-nitrilotris(N-(4-nitrophenyl)acetamide) (***H*$_3$*L*^{NO2}***): p-nitroaniline (12.1 g, 87.7 mmol) [excess aniline compound is critical], NTA (3.3 g, 17.4 mmol), pyridine (13.3 mL), triphenylphosphite (14.4 mL, 54.9 mmol). The final mixture was stirred for 2 days (45 hours total). After 2 days, the flask was allowed to cool to room temperature and diethyl ether (50 mL) was added and stirred for 90 minutes, yielding a light brown solid. The solid was isolated by filtration and then washed with chloroform (3 x 10 mL) and diethyl ether (2 x 10 mL) to yield a light tan solid (6.11 g, 63.7% based on NTA). ^{1}H NMR (DMSO-d_6, 300 MHz) δ 10.77 (3 H, s, N*H*), δ 8.16 (6 H, d, J = 8.8 Hz, o-C$_6$*H*$_6$), δ 7.81 (6 H, d, J = 8.8 Hz, m-C$_6$*H*$_6$), δ 3.70 (6 H, s, C*H*$_2$). ^{13}C NMR (DMSO-d_6, 400 MHz) δ 171.62, 145.29, 142.73, 125.50, 119.26, 59.08. ATR-FTIR (cm^{-1}): 3332, 3315, 3199, 3146, 3079, 2918, 1697, 1682, 1611, 1595, 1560, 1542. HRMS (MALDI/FT-ICR) m/z: [M - H]$^-$ Calcd for $C_{24}H_{20}N_7O_9$ 550.1328; Found 550.1359. The above procedure occasionally yielded intractable oils and therefore an alternative synthesis using nitrilotriacetyl chloride prepared *in situ* was developed. Nitrilotriacetic acid (1.48g, 7.7 mmol) was added to 15 ml of toluene in a 100 ml Schlenk flask and blanked with argon. To this mixture, excess thionyl chloride (5.2 ml, 72 mmol) was added dropwise at room temperature and refluxed overnight. The mixture was cooled to room temperature and the dark solution was treated with 15 ml of dichloromethane followed by slow addition of p-nitroaniline (3.32g, 24 mmol). The argon flow was stopped and a solution of Et_3N (7 mL) was added dropwise. The argon flow was returned and stirred at room temperature overnight. The solvent was removed and the resulting material boiled in methanol to give a light-brown solid that was filtered and washed with methanol. The resulting solid was then boiled in acetonitrile and filtered to yield a light brown solid (1.15 g, 27 %) with ^{1}H, ^{13}C NMR and ATR-FTIR that matched the product from the primary route described above.

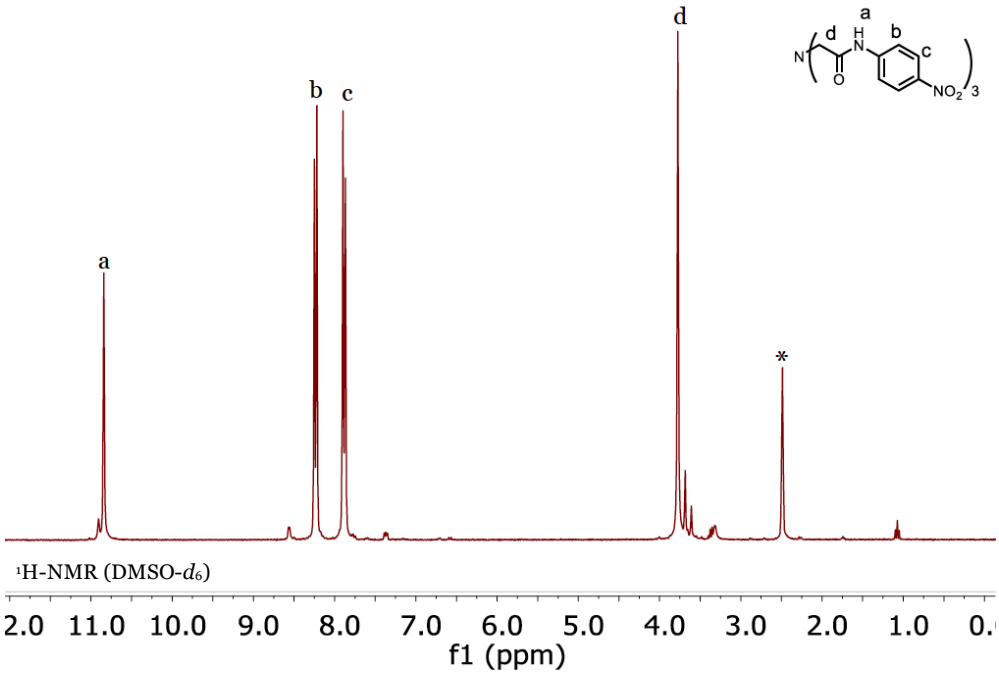

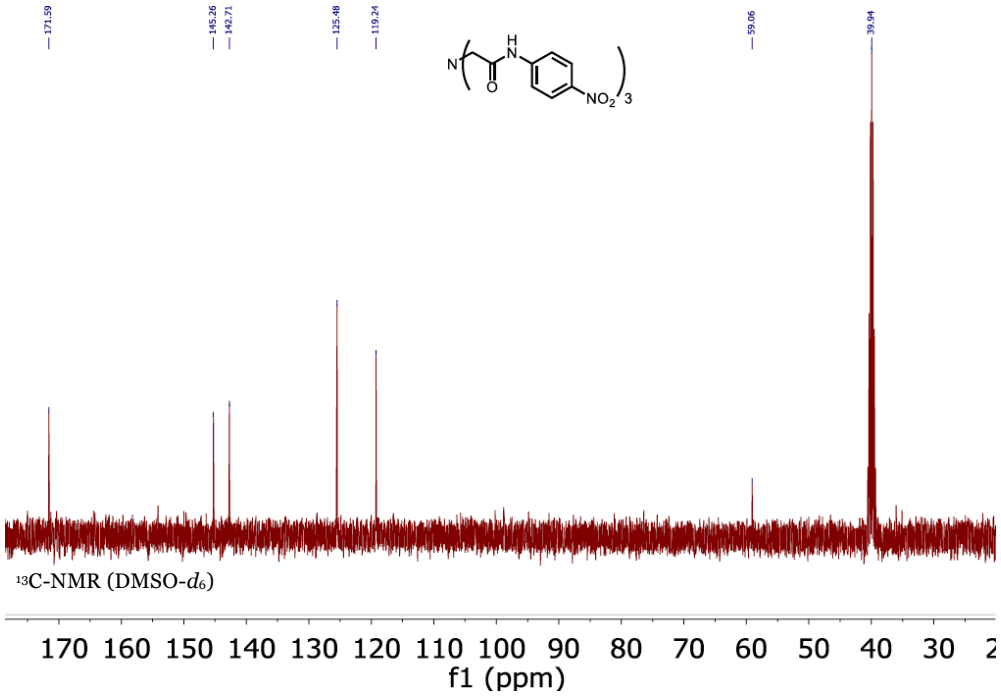

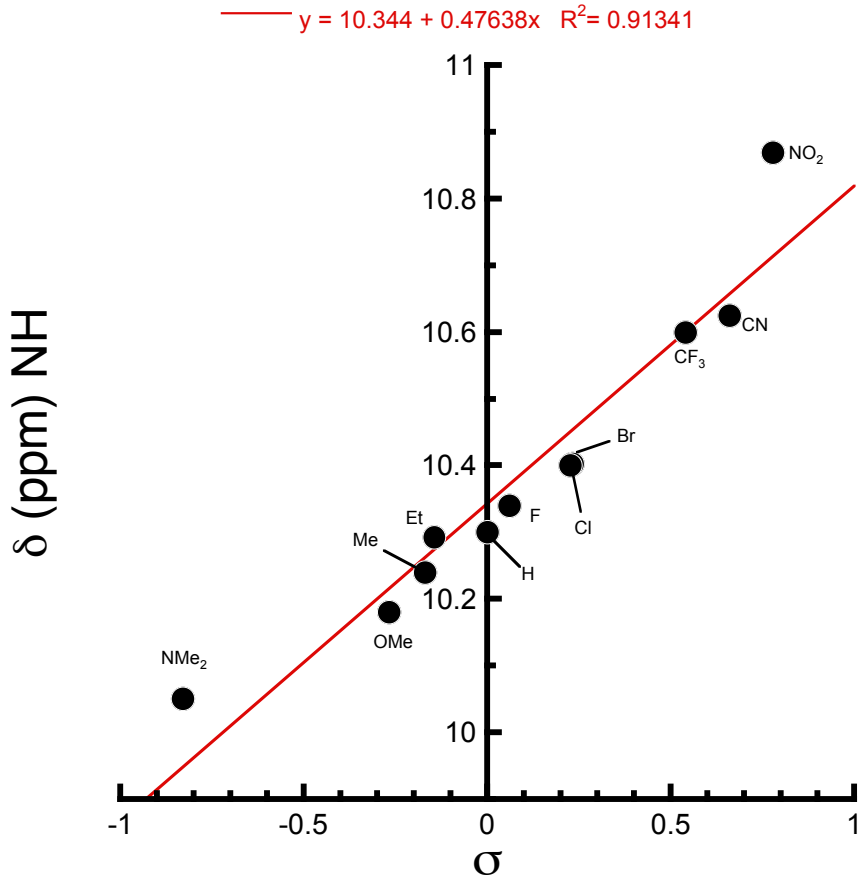

Figure S1. A plot of the [1]H-NMR obtained NH resonance of the tris-*N*-arylamide free ligands in DMSO (R designated for each point) against the Hammett sigma parameter.[2]

Metal complex synthesis

[Me_4N]$_2$[Fe$\mathbf{L^{NO2}}$(OAc)]: The ligand $\mathbf{H_3L^{NO2}}$ (100 mg, 0.18 mmol) was deprotonated with KH (22 mg, 0.56 mmol, 3.1 equiv.) in 2 mL of DMA in a 50 mL round bottom flask. After H_2 evolved ceased (≈ 10 minutes), $Fe(OAc)_2$ (33 mg, 0.19 mmol) was added and stirred for 15 minutes. Then two equivalents of [Me_4N][OAc] (48 mg, 0.36 mmol) were added followed by the addition of 1 ml of DMA that was used to wash all the reagents into the mixture. The resulting mixture was stirred at room temperature for 12 hours. The solution was then filtered through a glass fritted-funnel to remove insoluble material. The flask and solids in the glass frit were washed with 2 ml of DMA directly into filtrate. The filtrate was separated into 2 fractions and each fraction was layered under 12 to 15 ml of diethyl ether to obtain single crystals for XRD. (120 mg, 82% based on the ligand, $\mathbf{H_3L^{NO2}}$). ATR-FTIR (cm^{-1}): 3028, 2910, 1595, 1558, 1488, 1393, 1282, 1171, 1104, 940, 853, 744. Anal. Calcd for [Me_4N]$_2$[Fe$\mathbf{L^{NO2}}$(OAc)] $FeC_{35}H_{45}N_9O_{11}$: C, 50.32; H, 5.59; N, 15.53. Found: C, 50.21; H, 5.94; N, 15.39. HRMS (LDI/FT-ICR) m/z: Calcd for [Fe$\mathbf{L^{NO2}}$]$^-$ ($FeC_{24}H_{18}N_7O_9$) 604.0521; Found 604.0564. UV-vis: λ_{max} (DMA, nm (ε, M-1cm-1)) 266 (7570), 385 (28000), 485 (1540). Evans' method (DMSO-d_6, 298 K, 400 MHz NMR), μ_{eff} = 4.91 μ_B.

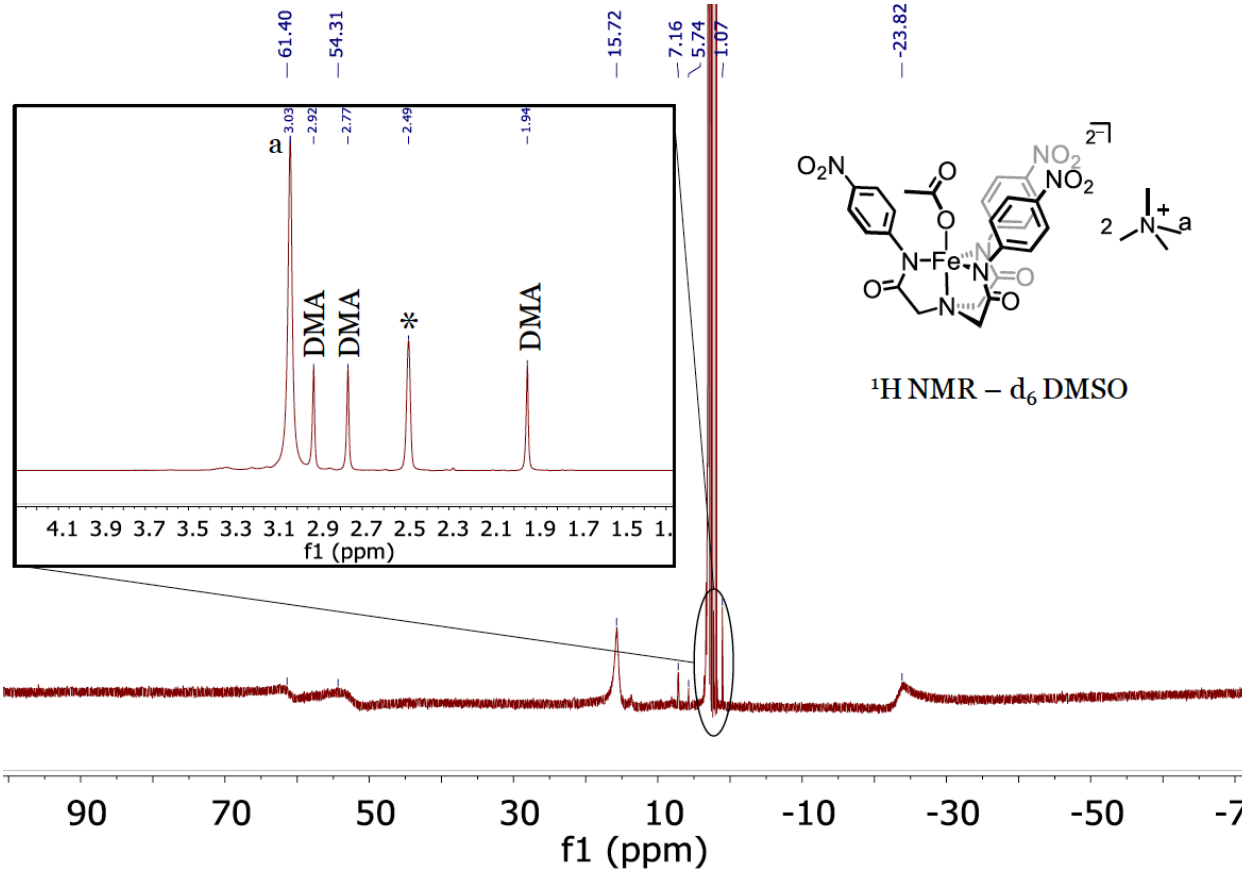

Figure S2a. ^{1}H-NMR [Me_4N]$_2$[Fe$\mathbf{L^{NO2}}$(OAc)] in DMSO-d_6 (* = NMR solvent).

[Me_4N]$_2$[Fe$\mathbf{L^H}$(OAc)]: The ligand $\mathbf{H_3L^H}$ (100 mg, 0.24 mmol) was deprotonated with KH (30 mg, 0.74 mmol) in 2 mL of DMA in a 50 mL round bottom flask. After H_2 evolved ceased (≈ 10 minutes), $Fe(OAc)_2$ (44 mg, 0.25 mmol) was added and stirred for 10 minutes. Then two equivalents of [Me_4N][OAc] (64 mg, 0.48 mmol) were added along with 1 ml of DMA, which was used to wash the sides of the vessel and the reaction was stirred at room temperature for 12 hours. The solution was then filtered through a glass frit to remove insoluble material. The reaction flask and solids on the frit were washed with 2 ml of DMA and added to the filtrate, which was layered under 12 to 15 ml of diethyl ether to yield crude product (130 mg, 80 % based on $\mathbf{H_3L^H}$). The crude product was filtered, washed with 2 ml of diethyl ether and dried on a glass frit. Once dry, the solid was dissolved in 3 ml of acetonitrile and slow diffusion of diethyl ether yielded crystalline material (77 mg, 47 % based on the ligand, $\mathbf{H_3L^H}$). ATR-FTIR (cm^{-1}): 3025, 2956, 2882, 2841, 1595, 1560. HRMS (LDI/FT-ICR) m/z: Calcd for [Fe$\mathbf{L^H}$]$^-$ ($FeC_{24}H_{21}N_4O_3$) 469.0969; Found 469.0985. Anal. Calcd for [Me_4N]$_2$[Fe$\mathbf{L^H}$(OAc)] ($C_{34}H_{48}FeN_6O_5$): C, 60.35; H, 7.15; N, 12.42. Found: C, 60.09; H, 7.09; N, 12.75.

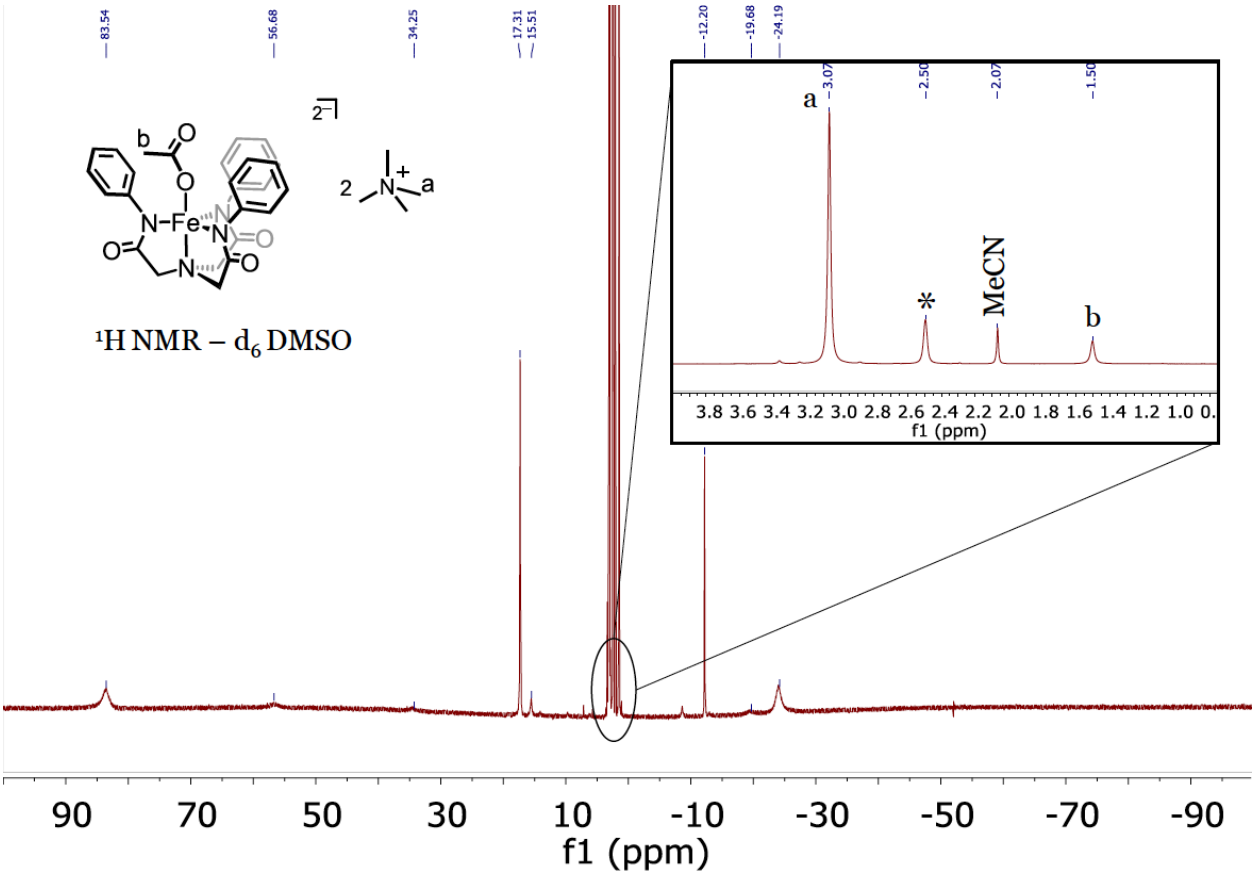

Figure S2b. ^{1}H-NMR [Me_4N]$_2$[Fe$\mathbf{L^H}$(OAc)] in DMSO-d_6 (* = NMR solvent).

Remainder of Fe^{II} compounds: The appropriate ligand ($\mathbf{H_3L^R}$) (100 mg, R = OMe, Et, H, F, Cl), was deprotonated with 3.1 molar equiv. KH in 2 mL of DMA in a 25-50 mL round bottom flask. After H_2 evolved ceased (≈ 10 minutes), one equivalent (slight excess 1.05 eq) of $Fe(OAc)_2$ was added and stirred for 10 minutes. Then two equivalents of $[Me_4N][OAc]$ were added along with 1 ml of dimethyl acetamide and the reaction was stirred at room temperature for 12 hours. The mixture was filtered through a glass frit to remove insoluble material. The flask and insoluble material was washed with 2 ml of DMA and passed through the frit directly into the filtrate. Recrystallization was accomplished by slow vapor diffusion or layering with diethyl ether. In some cases, an oily residue was obtained and triturated as described for the $[Me_4N]_2[Zn\mathbf{L^H}(OAc)]$ complex. The solid material was filtered, washed with diethyl ether and dried under vacuum. See Table below for characterization data for remaining iron complexes.

$[Me_4N]_2[Fe\mathbf{L^F}(OAc)]$: Yield = 55%. HRMS (LDI/FT-ICR) m/z: Calcd for $[Fe\mathbf{L^F}]^-$ 523.06859; Found 523.07052. ATR-FTIR (cm^{-1}): 3020, 2955, 2918, 2904, 1574, 1554, 1537, 1499. Anal. Calcd for $[Me_4N]_2[Fe\mathbf{L^F}(OAc)]$ ($C_{34}H_{45}F_3FeN_6O_5$): C, 55.89; H, 6.21; N, 11.50. Found: C, 54.98; H, 6.44; N, 11.01.

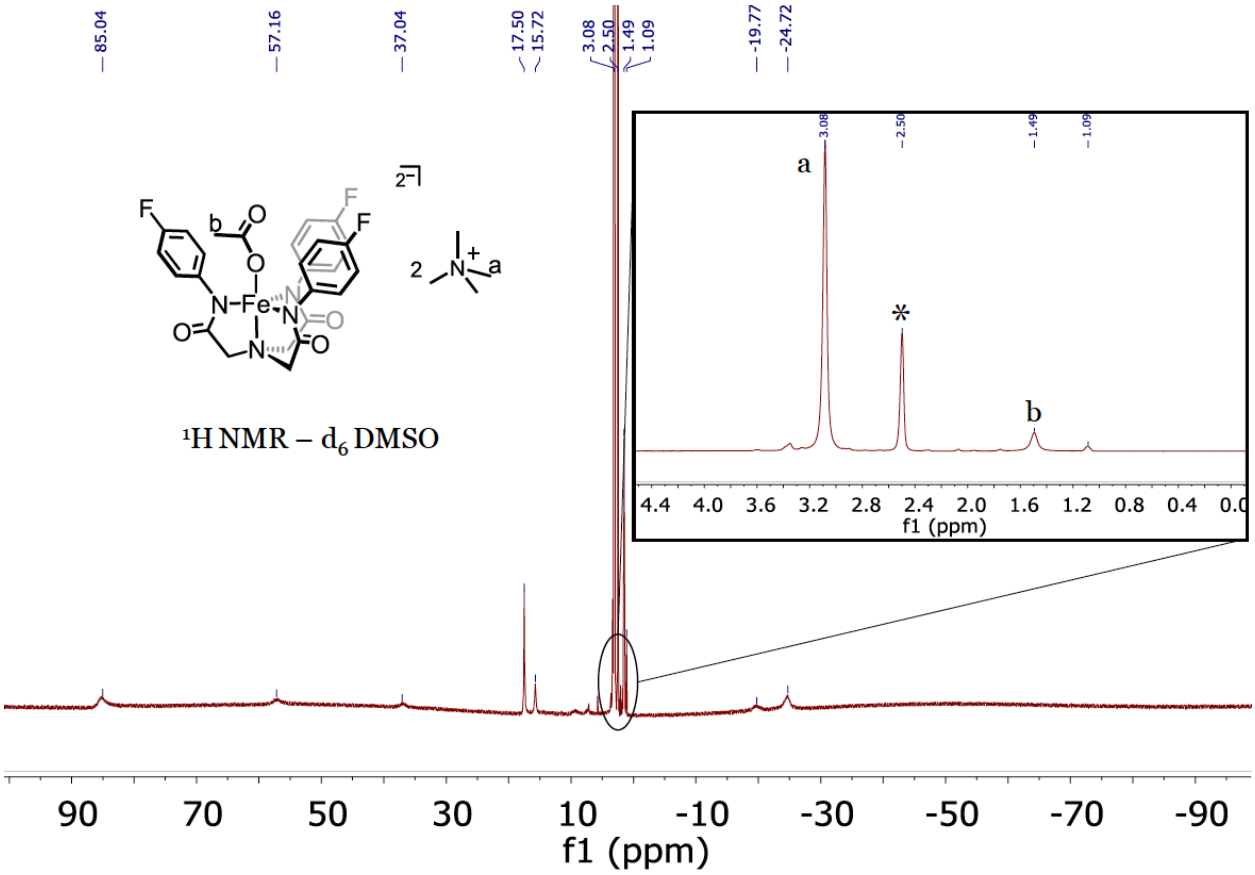

Figure 2c. ^{1}H-NMR $[Me_4N]_2[Fe\mathbf{L^F}(OAc)]$ in DMSO-d_6 (* = NMR solvent).

*[Me$_4$N]$_2$[Fe**L**^{Cl}(OAc)]*: Yield = 51%. HRMS (LDI/FT-ICR) m/z: Calcd for [Fe**L**^{Cl}]$^-$ 570.97993; Found 570.98229. ATR-FTIR (cm^{-1}): 3024, 2955, 2902, 2892, 2837, 1605, 1591, 1552, 1481. Anal. Calcd for [Me$_4$N]$_2$[Fe**L**^{Cl}(OAc)]•MeCN ($C_{36}H_{48}Cl_3FeN_7O_5$): C, 52.67; H, 5.89; N, 11.94. Found: C, 52.07; H, 6.42; N, 11.66. This batch was recrystallized from MeCN.

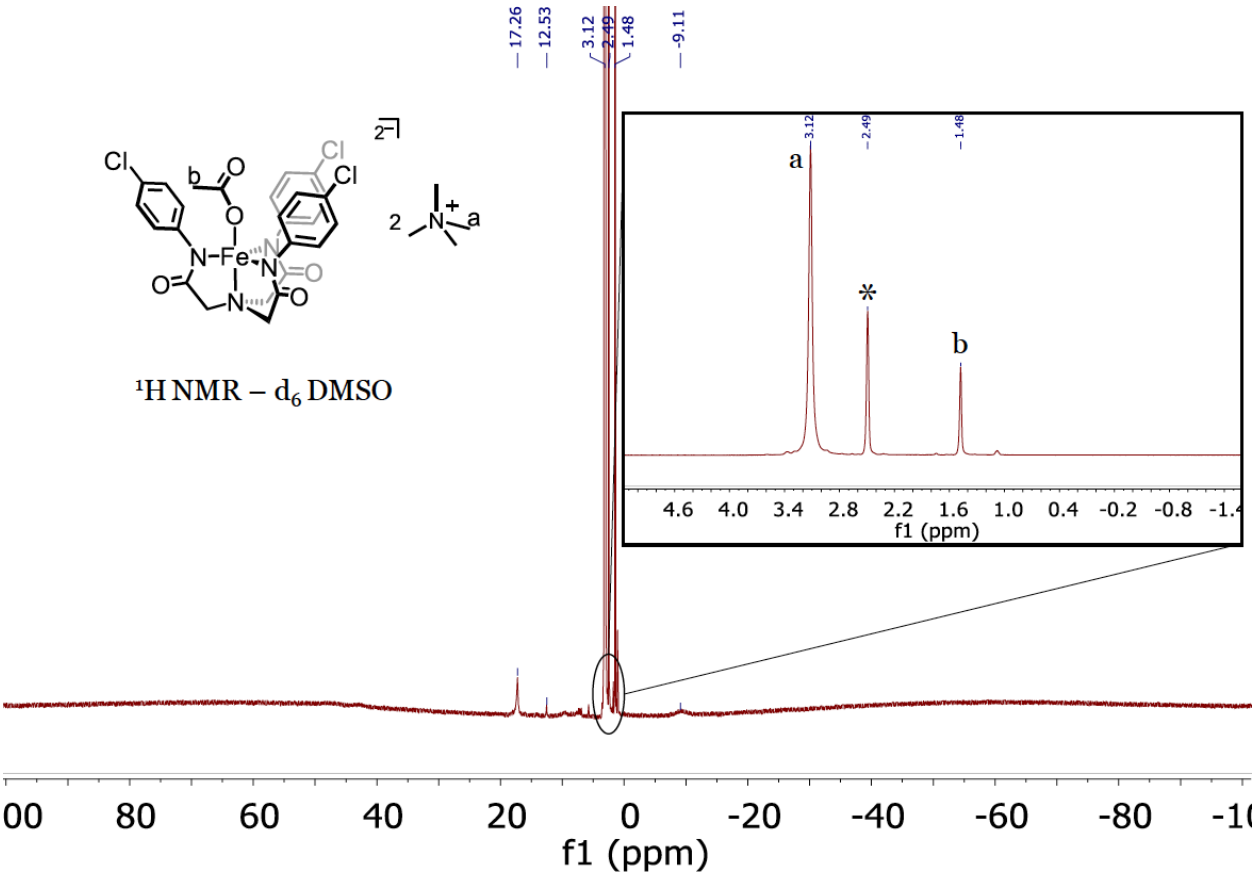

Figure 2d. ^{1}H-NMR [Me$_4$N]$_2$[Fe**L**^{Cl}(OAc)] in DMSO-d_6 (* = NMR solvent).

*[Me$_4$N]$_2$[Fe**L**^{OMe}(OAc)]*: Yield = 30%. HRMS (LDI/FT-ICR) m/z: Calcd for [Fe**L**^{OMe}]$^-$ 559.12855; Found 559.12931. ATR-FTIR (cm^{-1}): 3028, 2961, 2934, 2902, 2928, 1594, 1550, 1505, 1500, 1467. Anal. Calcd for [Me$_4$N]$_2$[Fe**L**^{OMe}(OAc)] ($C_{37}H_{54}FeN_6O_8$): C, 57.96; H, 7.10; N, 10.96. Found: C, 56.24; H, 8.83; N, 11.02.

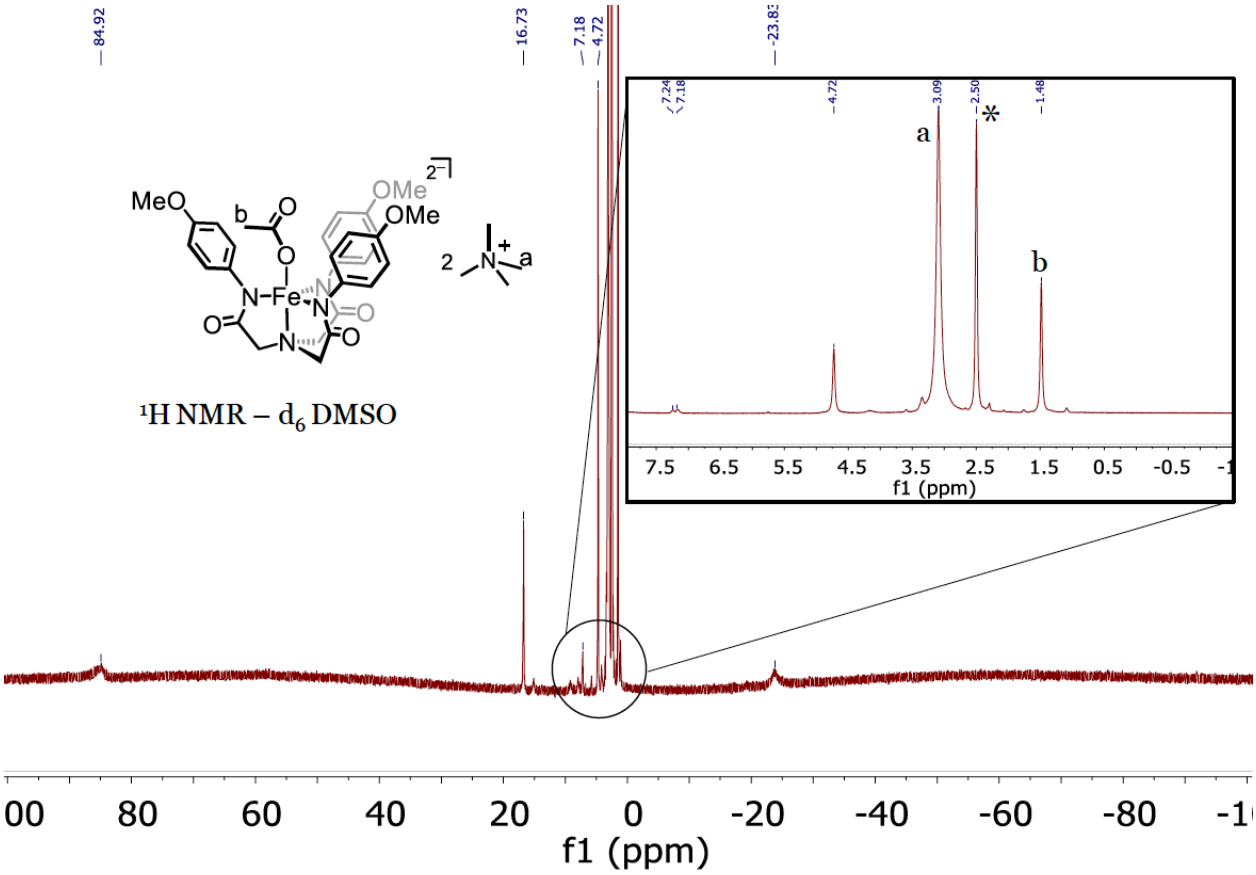

Figure S2e. ^{1}H-NMR [Me$_4$N]$_2$[Fe**L**^{OMe}(OAc)] in DMSO-d_6 (* = NMR solvent).

*[Me$_4$N]$_2$[Fe**L**^{Et}(OAc)]*: Yield = 82%. HRMS (LDI/FT-ICR) m/z: Calcd for [Fe**L**^{Et}]$^-$ 553.19075; Found 553.19243. ATR-FTIR (cm^{-1}): 3024, 2959, 2926, 2891, 2851, 1594, 1573, 1532, 1505, 1363. Anal. Calcd for [Me$_4$N]$_2$[Fe**L**^{Et}(OAc)] ($C_{40}H_{60}FeN_6O_5$): C, 63.15; H, 7.95; N, 11.05. Found: C, 62.97; H, 8.05; N, 11.01.

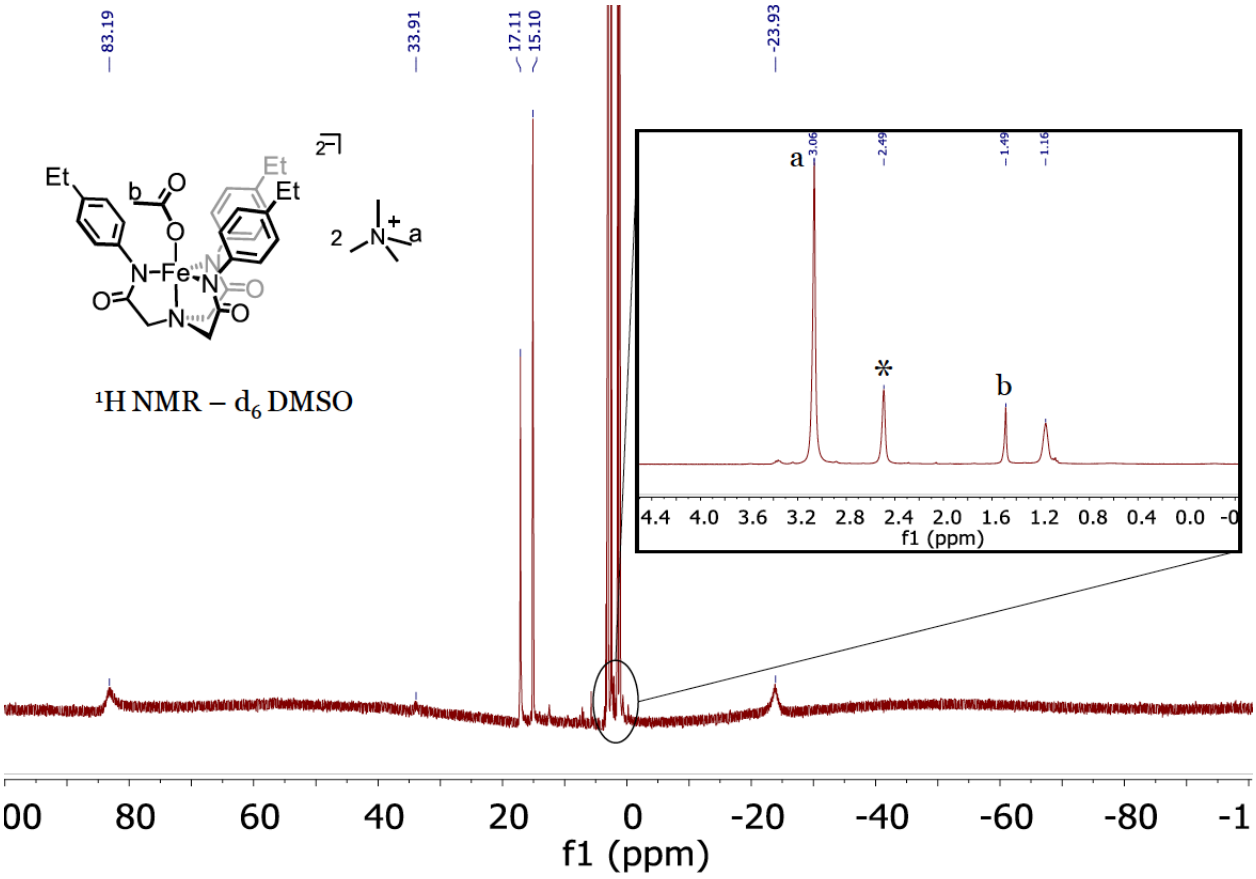

Figure S2f. ^{1}H-NMR [Me$_4$N]$_2$[Fe**L**^{Et}(OAc)] in DMSO-d_6 (* = NMR solvent).

*[Me$_4$N]$_2$[Zn**L**^{NO2}(OAc)]*: The ligand **H$_3$L^{NO2}** (100 mg, 0.181 mmol) was deprotonated with KH (22 mg, 0.544) in 2.0 mL of DMA in a 50 mL round bottom flask. After H_2 evolved ceased (≈10 minutes), $Zn(OAc)_2$ (33 mg, 0.18 mmol) was added and stirred for 10 minutes followed by one equivalent of [Me_4N][OAc] (24 mg, 0.18 mmol) and stirred for 24 h. The solution was then filtered through a glass frit to remove insoluble material. The filtrate was layered under diethyl ether to obtain crystals (82 mg, 67 % based on ligand). ATR-FTIR (cm^{-1}): 3025, 2919, 2819, 1632, 1562. ^{1}H-NMR (DMSO-d_6, 400 MHz, 298 K): δ 7.93 (6H, s, C*H*), δ 7.56 (6H, s, *CH)*, 3.13 (6H, s, *CH*), 3.09 (24H, s, *CH*), 0.95 (3H, s, *CH*). ^{13}C-NMR (DMSO-d_6, 300 MHz, 298 K): δ 172.71, 158.51, 140.29, 126.07, 123.43, 60.50, 54.80, 37.89, 34.93, 21.86. HRMS (LDI/FT-ICR) m/z: Calcd for [Zn**L**^{NO2}]$^-$ ($ZnC_{24}H_{18}N_7O_9$) 612.04629; Found 612.05179

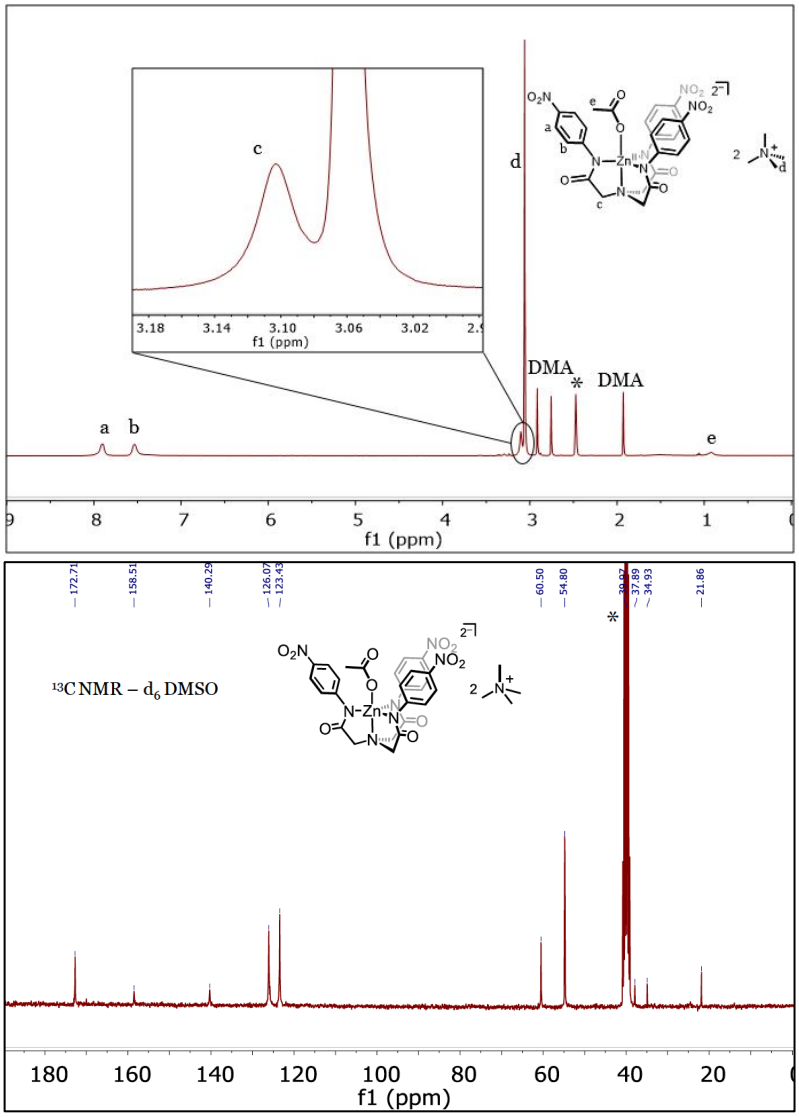

Figure S2g. ^{1}H-NMR (top) and ^{13}C-NMR of [Me_4N]$_2$[Zn**L**^{NO2}(OAc)] in DMSO-d_6 (* = NMR solvent).

[Me_4N]$_2$[Zn$\mathbf{L^H}$(OAc)]: The ligand $\mathbf{H_3L^H}$ (100 mg, 0.24 mmol) was deprotonated with KH (30 mg, 0.74 mmol) in 2 mL of DMA in a 25 mL round bottom flask. After H_2 evolved ceased (≈ 10 minutes), $Zn(OAc)_2$ (46 mg, 0.25 mmol) was added and stirred for 10 minutes. Then two equivalents of [Me_4N][OAc] (64 mg, 0.48 mmol) were added along with 1 ml of DMA, which was used to wash the sides of the vessel, and the reaction was stirred at room temperature for 12 hours. The solution was then filtered through a glass frit to remove insoluble material. The flask and insoluble material was washed with 1 ml of DMA and the filtrate is collected. The filtrate was layered under 12 to 15 ml of diethyl ether to yield a white oily residue. The mother liquor was decanted and the oil was triturated with 2 ml of diethyl ether and converted into a solid by scraping the vial with a spatula. The white solid was poured onto a glass frit, washed with diethyl ether, and dried on the frit under vacuum. Once dry, the solid on the frit was dissolved in 3 ml of acetonitrile and slow diffusion with diethyl ether yielded crystalline material (80 mg, 48 % based on ligand). ^{1}H-NMR (DMSO-d_6, 400 MHz, 298 K): δ 3.03 (s, 6H, –CH_2–), 3.06 (s, 24H, N(CH_3)$_4$), 6.81 (t, 3H, p-C_6H_6, J = 8 Hz), 7.02 (d, 6H, o-C_6H_6, J = 8 Hz), 7.09 (t, 6H, m-C_6H_6, J = 8 Hz). ^{13}C-NMR (DMSO-d_6, 400 MHz, 298 K): δ 171.41, 150.31, 127.70, 126.96, 121.45, 60.77, 54.82 (acetate carbons not observed). ATR-FTIR (cm^{-1}): 3024, 2956, 2916, 2877, 2834, 1597, 1577, 1556. HRMS (LDI/FT-ICR) m/z: Calcd for [Zn$\mathbf{L^H}$]$^-$ ($ZnC_{24}H_{21}N_4O_3$) 477.0911; Found 477.0918.

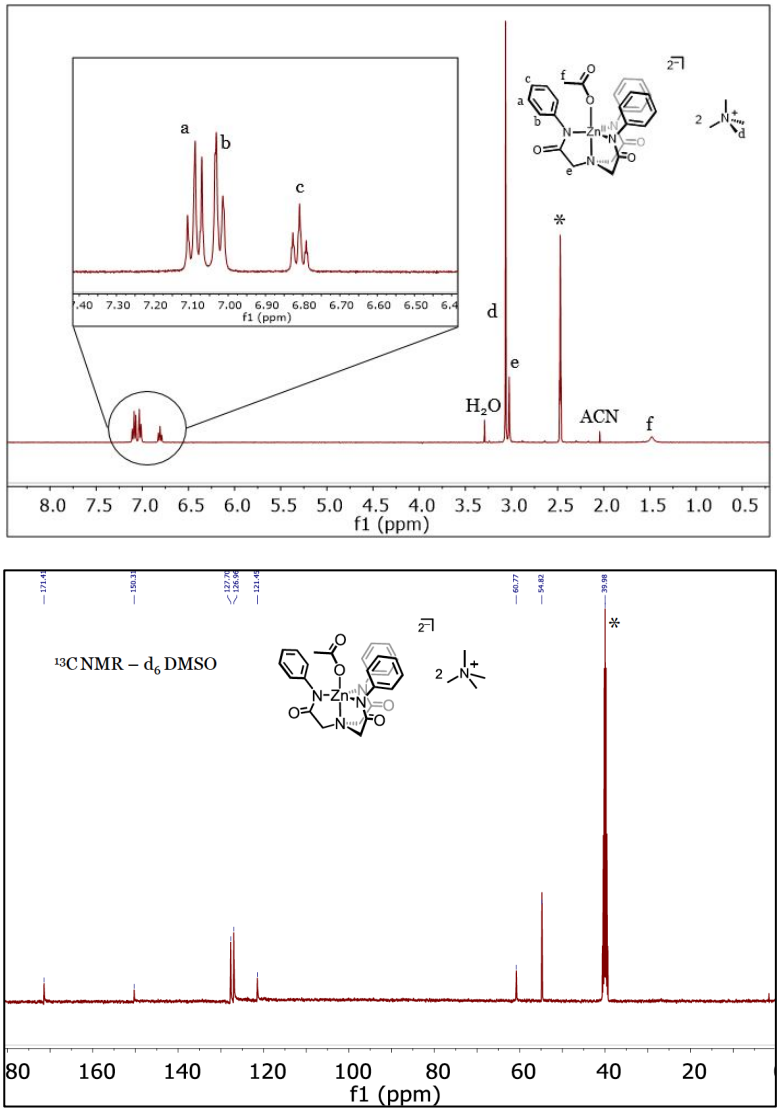

Figure S2h. ^{1}H-NMR (top) and ^{13}C-NMR (bottom) of [Me_4N]$_2$[Zn$\mathbf{L^H}$(OAc)] in DMSO-d_6 (* = NMR solvent).

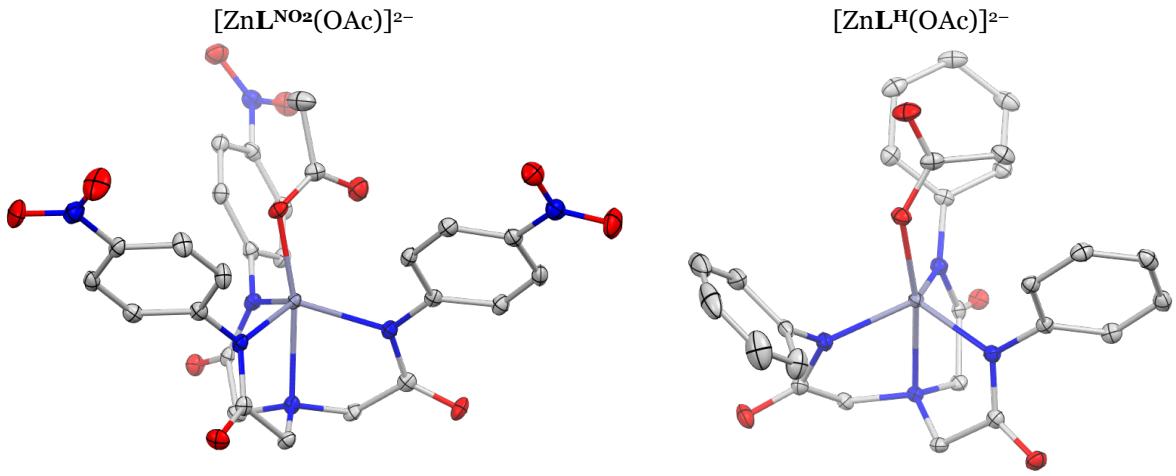

Figure S3. Molecular structure of the anions $[ZnL^{NO2}(OAc)]^{2-}$ and $[ZnL^{H}(OAc)]^{2-}$. Solvent molecules, counter ions, and hydrogen atoms have been removed for clarity. Ellipsoids are shown at the 50% probability level. Color scheme: blue/grey = zinc; blue = nitrogen; red = oxygen. See Table S1 for comparative bond metrics.

Table S1. Comparison of selected bond metrics for $[ML^{R}(OAc)]^{2-}$.

M^{R}	Fe^{NO2}	Zn^{NO2}	Fe^{H}	Zn^{H}
$M–N_{axial}$ (Å)	2.231(1)	2.243(2)	2.235(2)	2.252(2)
$M–N_{eq.\ ave}$ (Å)	2.158	2.102	2.105	2.066
$d[M–N_{eq.}]$ (Å)	0.543	0.493	0.486	0.456
$M–O_{short}$ (Å)*	2.111(1)	2.006(2)	2.046(1)	2.014(1)
$M–O_{long}$ (Å)*	2.456(2)	2.843(2)	4.218(2)	4.177(2)
$N–M–N_{ave}$ (°)	113.82	114.64	114.75	115.23
ionic radii (Å)	0.92	0.88	0.92	0.88

* O-atoms in acetate ligand

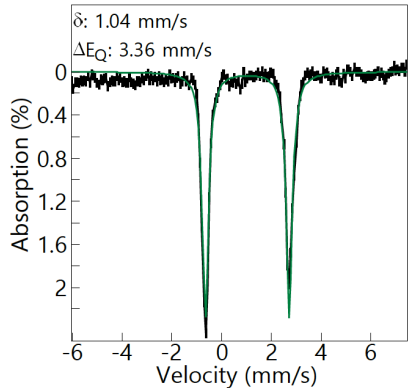

Figure S4. Mössbauer spectrum of $[FeL^{NO2}(OAc)]^{2-}$ (natural abundance ^{57}Fe, solid suspension in Nujol, 4.2 K)

Bulk oxidation of [Me$_4$N]$_2$[FeL^{NO2}(OAc)] with O$_2$.

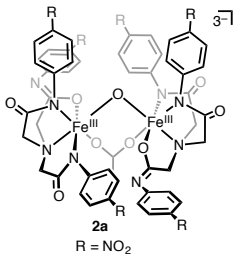

[Me$_4$N]$_3$[{Fe^{III}L^{NO2}}$_2$-(μ-O)-(μ-OAc)] (***2a***): In a glovebox, [Me$_4$N]$_2$[Fe**L**^{NO2}(OAc)] (50 mg, 0.062 mmol) was dissolved in 5 ml of DMA and transferred to a 100 mL Schlenk bomb. The flask was then sealed, removed from the glovebox and degassed on a Schlenk line *via* dynamic vacuum down to 130 mTorr. The flask was filled with pure O$_2$ (1 atm) and the solution was stirred for 1 hour. Upon addition of O$_2$ the homogenous solution changed color from a dark brown to red-yellow. After 1 hour, the solution was degassed again and the flask was brought back into the glovebox. The reaction mixture was separated into 2-3 equal portions and each was layered under 10 ml of diethyl ether to yield crystalline **2a** that was collected on a frit and washed thrice with 2 ml of diethyl ether (42 mg, 89 %). ATR-FTIR (cm^{-1}): 3024, 2954, 2909, 2825, 1594, 1562, 1515, 1488, 1393, 1303, 1282, 1235, 1171, 1104, 941, 918, 889, 865, 854, 839, 813, 756. UV-vis: λ_{max} (DMA, nm (ε, M^{-1} cm^{-1})) 285 (32500), 359 (49300). Anal. Calcd (Found) for [Me$_4$N]$_3$[{Fe^{III}L^{NO2}}$_2$-(μ-O)-(μ-OAc)] ($C_{62}H_{75}Fe_2N_{17}O_{20}$): C, 49.98 (49.53); H, 5.07 (5.50); N, 15.98 (15.60). Magnetic moment μ_{eff} = 3.01 μ_B (DMSO-d_6, Evans' method, 295 K).

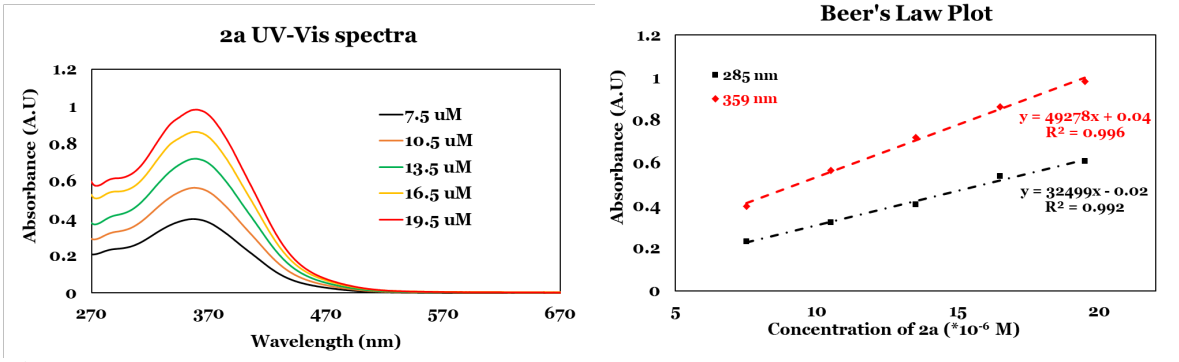

Figure S5a. UV-vis spectrum of **2a** in DMA at various concentration (left) with corresponding Beer's law plot for extinction coefficient (right).

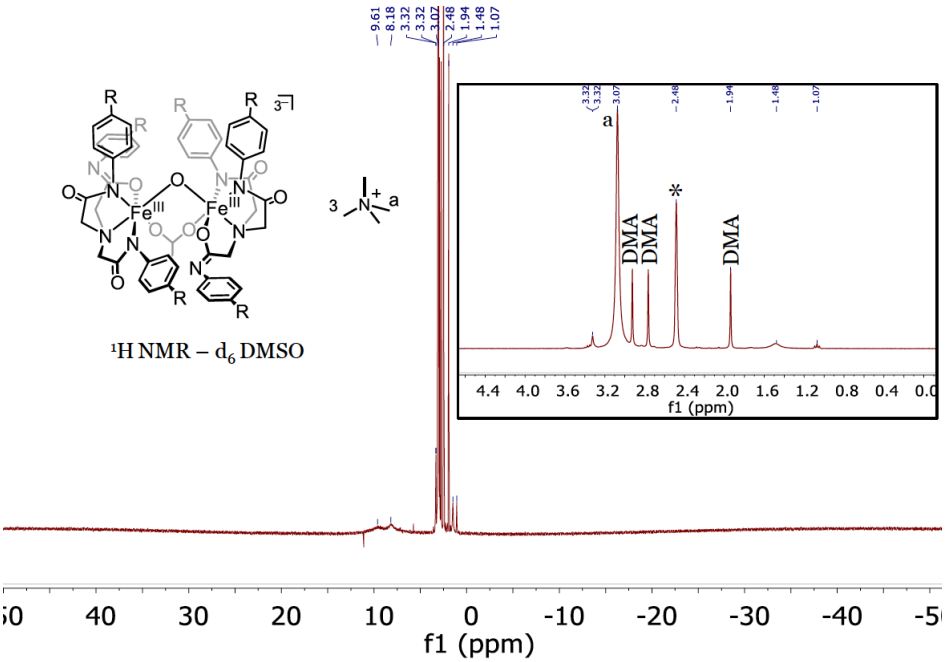

Figure S5b. ^{1}H-NMR of **2a** in DMSO-d_6 (* = NMR solvent).

*[Me$_4$N]$_2$[{Fe^{III}**L^{NO2}**}$_2$-μ-O]* (***2b***): In a glovebox, [Me$_4$N]$_2$[FeL^{NO2}(OAc)] (50 mg, 0.062 mmol) was dissolved in 5 ml of acetonitrile and transferred to a 100 mL Schlenk bomb. The flask was then sealed, removed from the glovebox and degassed on a Schlenk line *via* freeze pump thaw cycles. The flask was filled with pure O_2 (1 atm) and the solution was stirred for 1 hour. Upon addition of O_2 the homogenous solution changed color from a dark brown to golden brown. After 1 hour, the solution was degassed again *via* freeze pump thaw and the flask was brought back into the glovebox. The reaction mixture was separated into 2-3 equal portions and each was layered under 10 ml of diethyl ether to yield crystalline **2b** that was collected on a frit and washed thrice with 2 ml of diethyl ether (37 mg, 88 %). ATR-FTIR (cm^{-1}): 3032, 2958, 2910, 2894, 2823, 1595, 1560, 1539, 1516, 1484, 1391, 1285, 1168, 1104, 943, 914, 888, 852, 756. UV-vis: λ_{max} (MeCN, nm (ε, M^{-1} cm^{-1})) 286 (20700), 343 (32100), 487 (1900). UV-vis: λ_{max} (DMA, nm (ε, M^{-1} cm^{-1})) 358 (51900). Magnetic moment μ_{eff} = 2.26 μ_B (DMSO-*d*$_6$, Evans' method, 295 K).

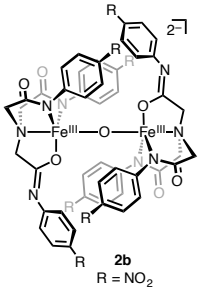

Despite our best efforts, CHN data was always slightly off. CHN analyses were collected on two separate batches (NMR spectra for both batches below). Batch 1: C, 48.36; H, 5.46; N, 14.54. Batch 2: C, 49.03; H, 5.65; N, 14.54. The theoretical CHN for [Me$_4$N]$_2$[{Fe^{III}**L^{NO2}**}$_2$-μ-O (C$_{56}$H$_{60}$Fe$_2$N$_{16}$O$_{19}$) is: C, 48.99; H, 4.41; N, 16.32.

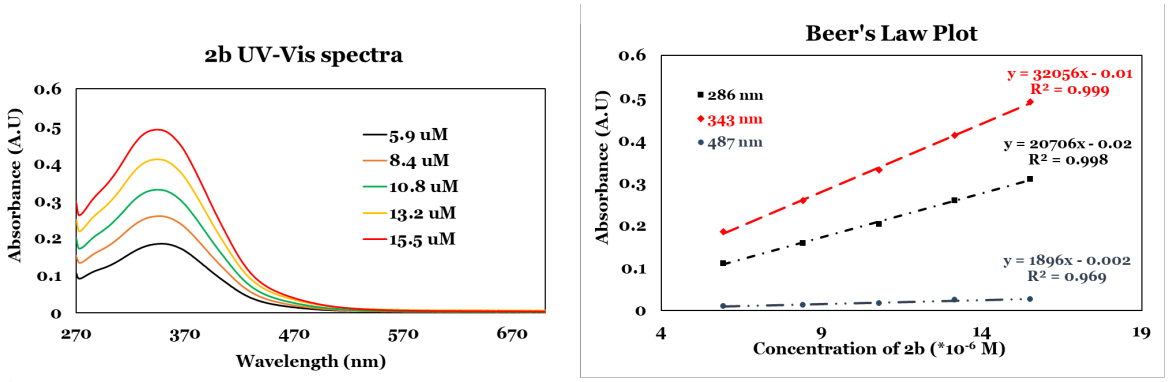

Figure S5c. UV-vis spectrum of **2b** in MeCN at various concentration (left) with corresponding Beer's law plot for extinction coefficient (right).

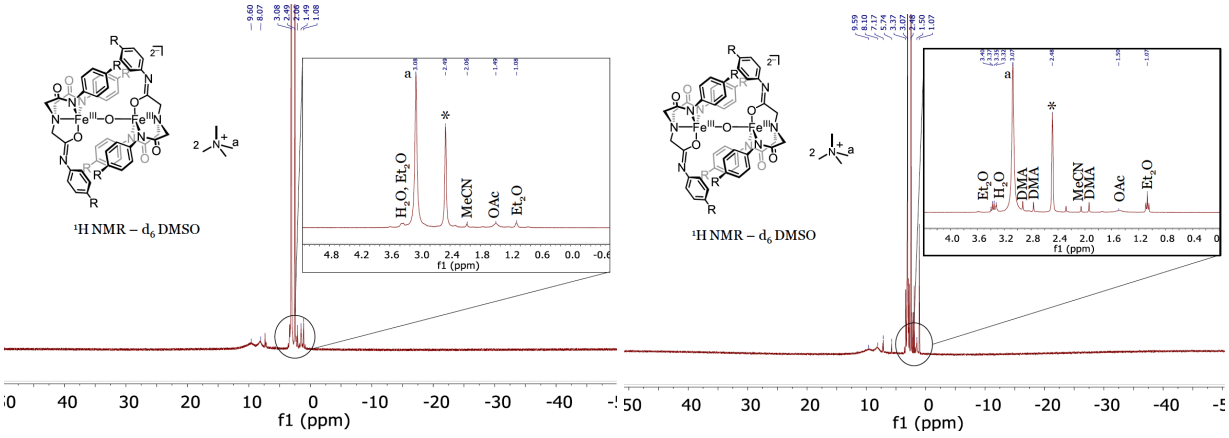

Figure S5d. ^{1}H-NMR of **2a** in DMSO-*d*$_6$ (* = NMR solvent). Sample used to prepare CHN batch 1, left. Sample used to prepare CHN batch 2, right.

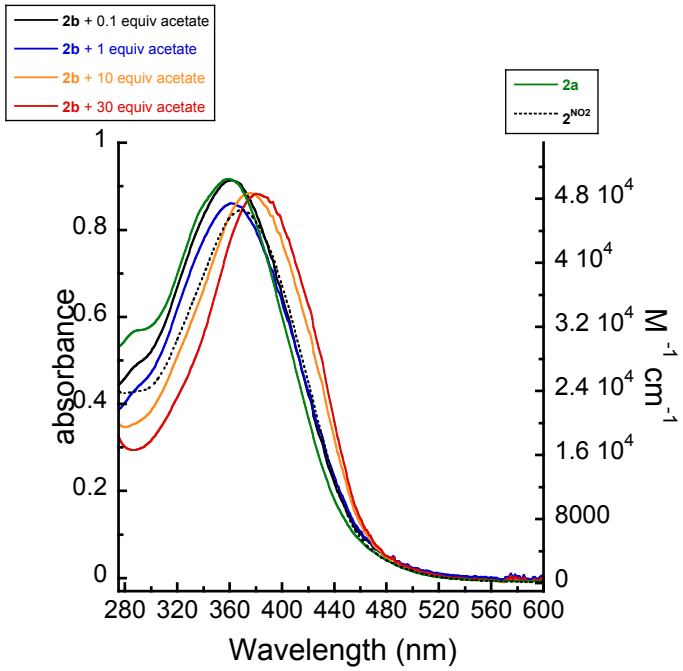

Figure S6. Comparison of $\mathbf{2}^{NO2}$ (black dotted line) generated at low concentration (0.1 to 0.5 mM) by treatment of $\mathbf{1}^{NO2}$ with excess O_2 in a cuvette with as isolated **2a** (green) and **2b** (black, with 0.1 equiv additional acetate). Three other solutions of **2b** with added acetate are shown; blue = 1 equiv acetate, orange = 10 equiv acetate, and red = 30 equiv acetate. Spectra were obtained in DMA at rt.

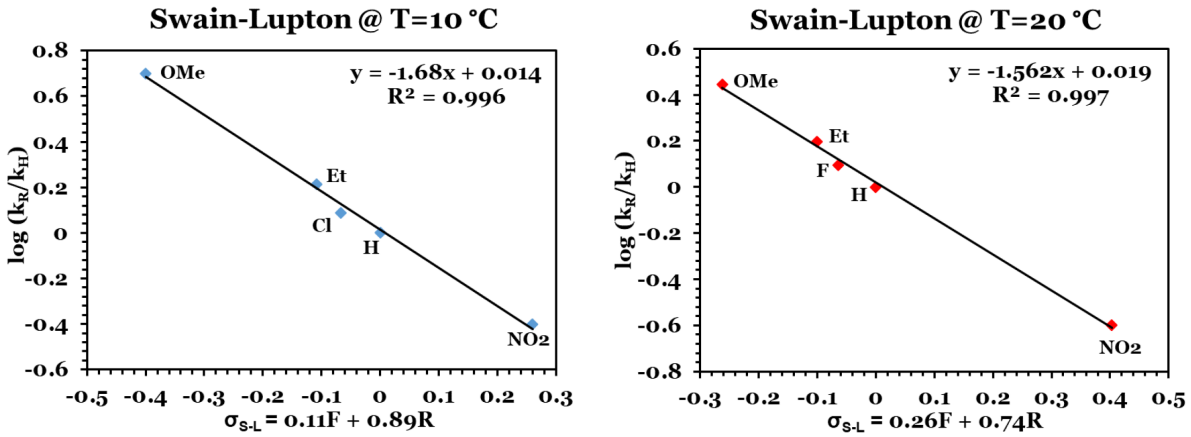

Figure 7a. Swain-Lupton plots at 10 °C (left) and 20 °C (right – same as Figure 5 in manuscript) in DMA.

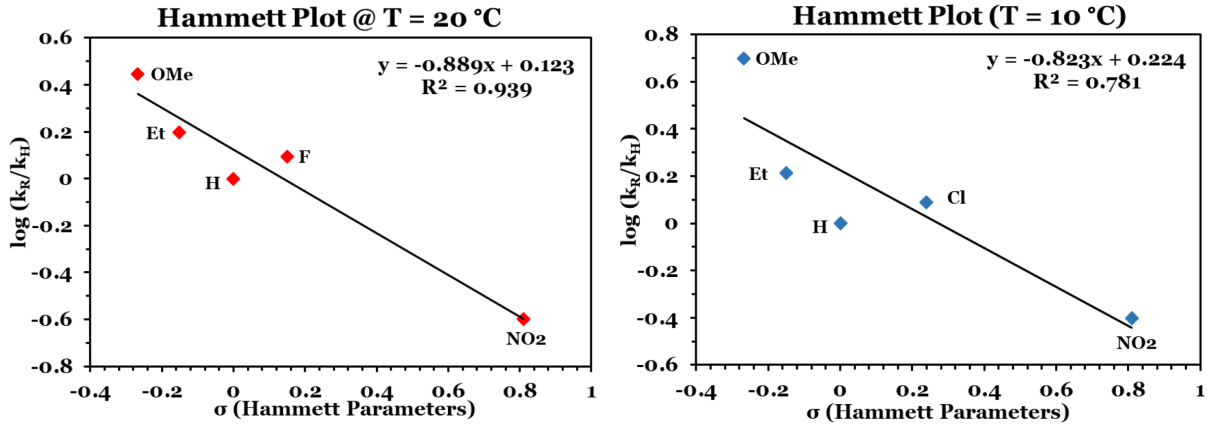

Figure 7b. Hammett plots at 10 °C (left) and 20 °C (right) in DMA.

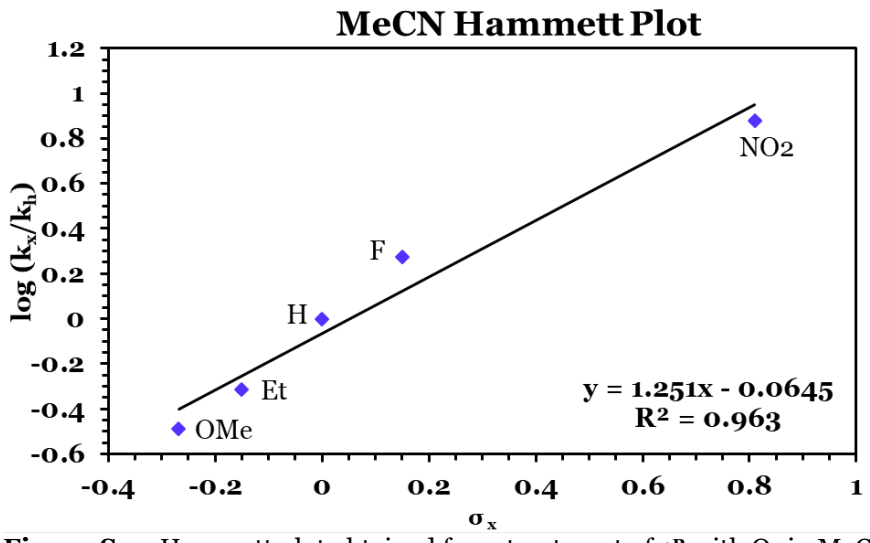

Figure S7c. Hammett plot obtained from treatment of $\mathbf{1^R}$ with O_2 in MeCN at 20 °C.

Derivation of rate law for O_2 reduction with $\mathbf{1^R}$

For the mechanism in Scheme 3 of the manuscript…

$$-\frac{d[Fe\boldsymbol{L^R}(OAc)]}{dt} = k_1[Fe\boldsymbol{L^R}(OAc)] - k_{-1}[Fe\boldsymbol{L^R}][\mathrm{OAc}] \qquad \textit{equation S1}$$

$$\frac{d[Fe\boldsymbol{L^R}]}{dt} = k_1[Fe\boldsymbol{L^R}(OAc)] - k_{-1}[Fe\boldsymbol{L^R}][\mathrm{OAc}] - k_2[Fe\boldsymbol{L^R}][\mathrm{O_2}] \qquad \textit{equation S2}$$

$$\frac{d[\mathbf{2}]}{dt} = k_2[Fe\boldsymbol{L^R}][\mathrm{O_2}] \qquad \textit{equation S3}$$

Assuming the **steady state approximation** (setting the second equation equal to zero) provides the rate law presented in the manuscript.

$$\frac{d[\mathbf{2}]}{dt} = \frac{k_1k_2[Fe\boldsymbol{L^R}(OAc)][O_2]}{k_{-1}[OAc]+k_2[O_2]} \qquad \textit{equation S4}$$

A plot of $1/k_{obs}$ plotted against $1/[O_2]$ provides y intercept = $1/k_1$ and the slope = k'

$$k_{obs} = \frac{k_1k_2[O_2]}{k_{-1}[OAc]+k_2[O_2]} \qquad \textit{equation S5}$$

$$\frac{1}{k_{obs}} = \frac{k_{-1}[OAc]}{k_1k_2[O_2]} + \frac{1}{k_1} \qquad \textit{equation S6}$$

$$k' = \frac{k_{-1}[OAc]}{k_1k_2} \qquad \textit{equation S7}$$

considering K_{eq} and the following I.C.E. tables...

$$\mathrm{K}_{eq} = \frac{k_1}{k_{-1}} = \frac{[Fe\boldsymbol{L^R}][\mathrm{OAc}]}{[Fe\boldsymbol{L^R}(OAc)]} \qquad \textit{equation S8}$$

	$[\mathrm{Fe(OAc)}\mathbf{L^R}]_t$	$[\mathrm{Fe}\mathbf{L^R}]_t$	$[\mathrm{OAc}]_t$
initial conc.	$[\mathrm{Fe(OAc)}\mathbf{L^R}]_0$ = 0.1 mM	0	0
change in conc.	- $[\mathrm{OAc}]_{eq}$	$[\mathrm{OAc}]_{eq}$	$[\mathrm{OAc}]_{eq}$
equilibrium conc.	$[\mathrm{Fe(OAc)}\mathbf{L^R}]_0 - [\mathrm{OAc}]_{eq}$	$[\mathrm{OAc}]_{eq}$	$[\mathrm{OAc}]_{eq}$
perturbation to equilibrium	0	0	$[\mathrm{OAc}]_{added}$
new change	$[\mathrm{OAc}]_p$	-$[\mathrm{OAc}]_p$	-$[\mathrm{OAc}]_p$
final equilibrium	$[\mathrm{Fe(OAc)}\mathbf{L^R}]_0$ - $[\mathrm{OAc}]_{eq}$ + $[\mathrm{OAc}]_p$	$[\mathrm{OAc}]_{eq}$ - $[\mathrm{OAc}]_p$	$[\mathrm{OAc}]_{eq}$ + $[\mathrm{OAc}]_{added}$ - $[\mathrm{OAc}]_p$

$$\mathrm{K}_{eq} = \frac{k_1}{k_{-1}} = \frac{([\mathrm{OAc}]_{eq} - [\mathrm{OAc}]_p)([\mathrm{OAc}]_{eq} + [\mathrm{OAc}]_{added} - [\mathrm{OAc}]_p)}{([Fe\boldsymbol{L^R}(OAc)]_0 - [\mathrm{OAc}]_{eq} + [\mathrm{OAc}]_p)} = \frac{[\mathrm{OAc}]_{eq}^2}{([Fe\boldsymbol{L^R}(OAc)]_0 - [\mathrm{OAc}]_{eq})} \qquad \textit{equation S9}$$

and substituting the K_{eq} and final equilibrium acentate concentration for $[\mathrm{OAc}]_t$ back into the equation for k'

$$k' = \frac{k_{-1}[OAc]_t}{k_1k_2} = \frac{[OAc]_t}{K_{eq}k_2} = \frac{[Fe\boldsymbol{L^R}(OAc)]_0 - [\mathrm{OAc}]_{added} + [\mathrm{OAc}]_p}{[\mathrm{OAc}]_{added} - [\mathrm{OAc}]_p} * \frac{1}{k_2} \qquad \textit{equation S10}$$

Next, a plot of $1/k_{obs}$ against $1/[O_2]$ was obtained for two different values of $[\mathrm{OAc}]_{added}$ with constant $[\mathrm{Fe(OAc)}\mathbf{L^R}]_0$ and $[\mathrm{OAc}]_{eq}$

$[\mathrm{OAc}]_{added}$ = 20*$[\mathrm{Fe(OAc)}\mathbf{L^R}]_0$ = $[\mathrm{OAc}]_{20}$ and is associated with k'_{20} and $[\mathrm{OAc}]_{p20}$

$[\mathrm{OAc}]_{added}$ = 30*$[\mathrm{Fe(OAc)}\mathbf{L^R}]_0$ = $[\mathrm{OAc}]_{30}$ and is associated with k'_{30} and $[\mathrm{OAc}]_{p30}$

Value k_2 and $[OAc]_{eq}$ remain the same. Hence, we now have a system of four equations and four unknowns (k_2, $[OAc]_{eq}$, $[OAc]_{p20}$, and $[OAc]_{p30}$)…

System Equation 1: $$k'_{20} = \frac{[Fe\boldsymbol{L^R}(OAc)]_0 - [OAc]_{eq} + [OAc]_{p20}}{[OAc]_{eq} - [OAc]_{p20}} * \frac{1}{k_2}$$ *equation S11*

System Equation 2: $$\frac{([OAc]_{eq} - [OAc]_{p20})([OAc]_{eq} + [OAc]_{20} - [OAc]_{p20})}{([Fe\boldsymbol{L^R}(OAc)]_0 - [OAc]_{eq} + [OAc]_{p20})} = \frac{[OAc]_{eq}^2}{([Fe\boldsymbol{L^R}(OAc)]_0 - [OAc]_{eq})}$$ *equation S12*

System Equation 3: $$k'_{30} = \frac{[Fe\boldsymbol{L^R}(OAc)]_0 - [OAc]_{eq} + [OAc]_{p30}}{[OAc]_{eq} - [OAc]_{p30}} * \frac{1}{k_2}$$ *equation S13*

System Equation 4: $$\frac{([OAc]_{eq} - [OAc]_{p30})([OAc]_{eq} + [OAc]_{30} - [OAc]_{p30})}{([Fe\boldsymbol{L^R}(OAc)]_0 - [OAc]_{eq} + [OAc]_{p30})} = \frac{[OAc]_{eq}^2}{([Fe\boldsymbol{L^R}(OAc)]_0 - [OAc]_{eq})}$$ *equation S14*

The inbuilt non-linear solver "*fsolve*" in MATLAB was used to obtain values for k_2 and the concentrations $[OAc]_{eq}$, $[OAc]_{p20}$, and $[OAc]_{p30}$. The values below are an estimate that is accurate to the order or magnitude presented due to the tolerance set in the MATLAB code.

$k_2 = 0.39\ M^{-1}\cdot s^{-}$

$[OAc]_{eq} = 9.97\text{x}10^{-5}$ M

$[OAc]_{p20} = 2.3\text{x}10^{-6}$ M

$[OAc]_{p30} = 3.9\text{x}10^{-6}$ M

These allow one to calculate the value of K_{eq} (0.08) and subsequently k_{-1} 0.27 $M^{-1}\cdot s^{-1}$.

An alternative **prior equilibrium** approach provides a different rate law…

$$K_{eq} = \frac{k_1}{k_{-1}} = \frac{[Fe\boldsymbol{L^R}]_{eq}[OAc]_{eq}}{[Fe\boldsymbol{L^R}(OAc)]_{eq}}$$ *equation S15*

$$[Fe\boldsymbol{L^R}(OAc)]_{eq} = [Fe\boldsymbol{L^R}(OAc)]_0 - [Fe\boldsymbol{L^R}]_{eq}$$ *equation S16*

$$\frac{d[\mathbf{2}]}{dt} = \frac{k_1 k_2 [Fe\boldsymbol{L^R}(OAc)][O_2]}{k_{-1}[OAc] + k_1}$$ *equation S17*

Another alternative approach arises when one considers that the 5-coordinate complex [Fe(OAc)$\mathbf{L^R}$] reacts with O_2, two other rate laws are possible; neither of these rate laws explain the observed trends.

Assume steady state for [Fe(OAc)$\mathbf{L^R}$] $$\frac{d[\mathbf{2}]}{dt} = \frac{k_{-1}k_2[Fe\boldsymbol{L^R}][OAc][O_2]}{k_2[O_2] + k_1}$$ *equation S18*

Assume steady state for [Fe$\mathbf{L^R}$] $$\frac{d[\mathbf{2}]}{dt} = \frac{k_1 k_2 [Fe\boldsymbol{L^R}(OAc)][O_2]}{k_{-1}[OAc]}$$ *equation S19*

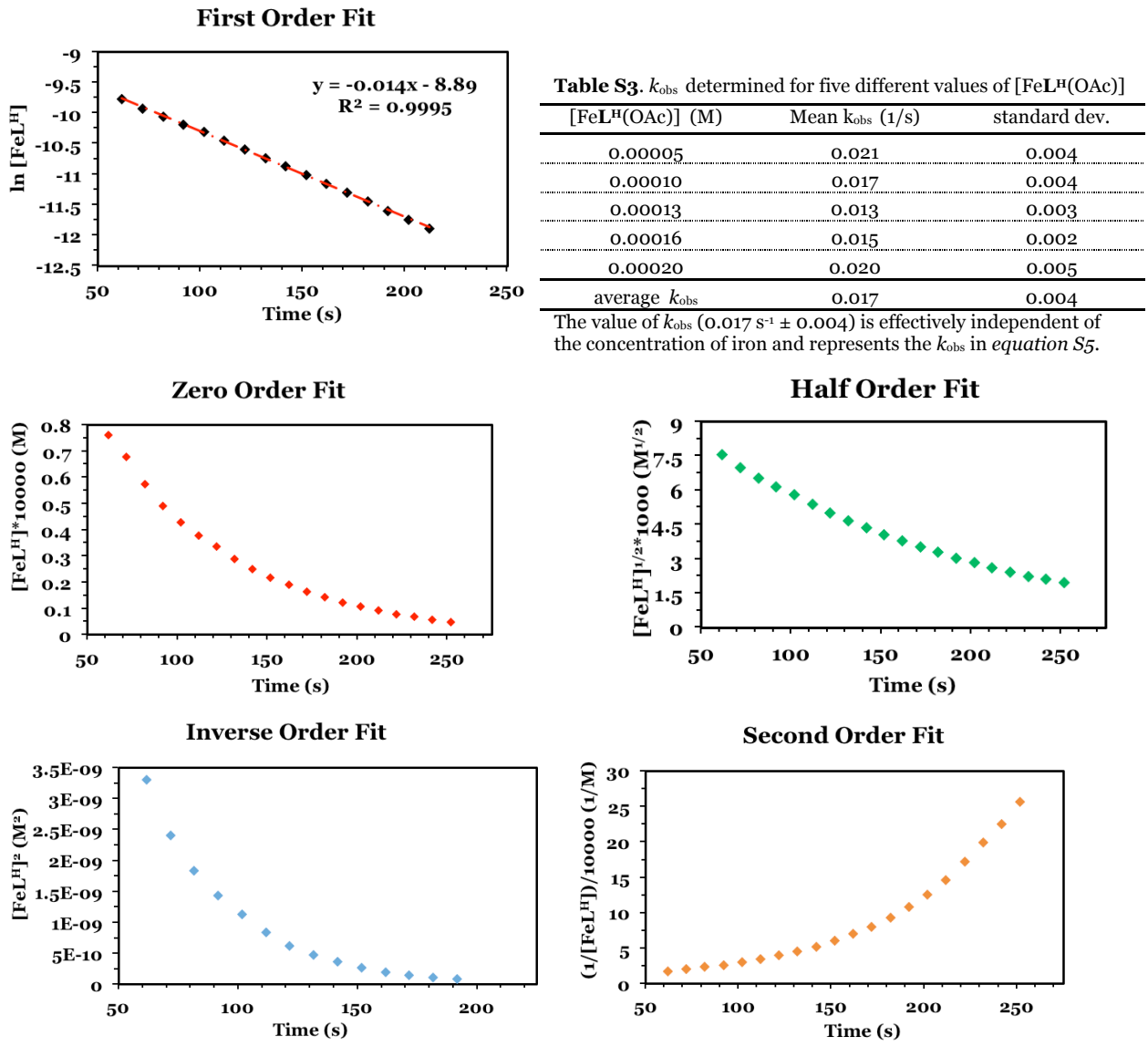

Table S3. k_{obs} determined for five different values of [Fe**L**^{H}(OAc)]

[Fe**L**^{H}(OAc)] (M)	Mean k_{obs} (1/s)	standard dev.
0.00005	0.021	0.004
0.00010	0.017	0.004
0.00013	0.013	0.003
0.00016	0.015	0.002
0.00020	0.020	0.005
average k_{obs}	0.017	0.004

The value of k_{obs} (0.017 s^{-1} ± 0.004) is effectively independent of the concentration of iron and represents the k_{obs} in *equation S5*.

Figure S8. Representative plots (0.1 mM) for order determination of iron in O_2 reduction mechanism with **1**^{H} in DMA. The iron concentration was varied (0.050 mM, 0.10 mM, 0.13 mM, 0.16 mM, 0.2 mM) and treated with 0.75 atm O_2 at 20 °C. Each concentration was repeated in triplicate and the linearized integrated rate expressions were plotted. The first order plot provided the best fit (shown upper left) with data from the five concentrations (shown upper right).

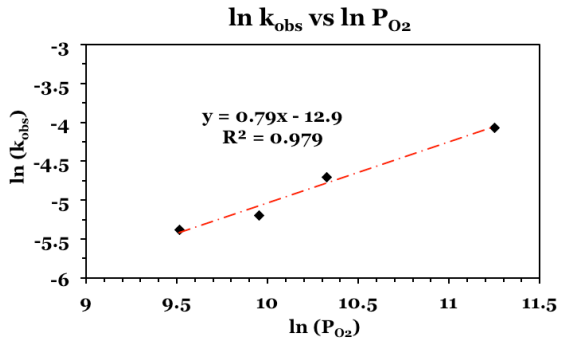

Figure S9. Representative plot for order determination of $[O_2]$ in $\mathbf{1^H}$ mediated O_2 reduction.

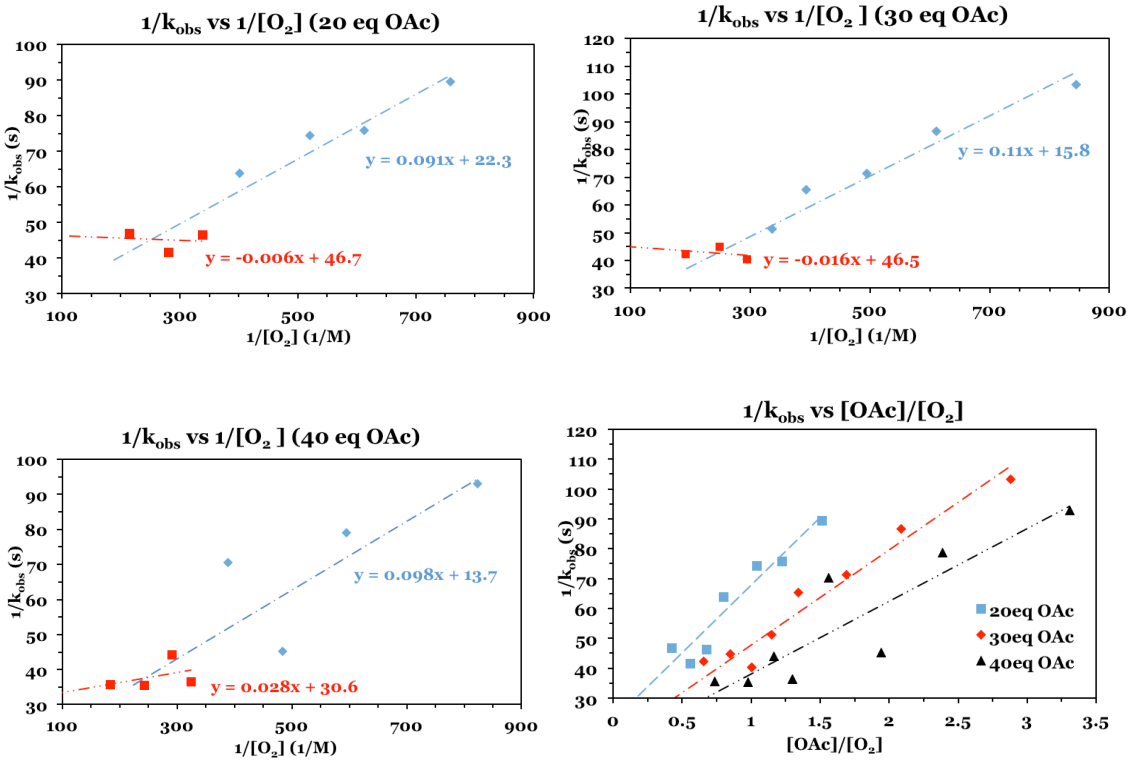

Figure S10. Plot of $1/k_{obs}$ vs. $1/[O]_2$ for $\mathbf{1^H}$ (0.1 mM) with 20, 30, and 40 equiv of $[Me_4N][OAc]$ in DMA. The *y*-intercept in the horizontal region (red) is $1/k_1$ (*equation S6*) and slope for the low $[O_2]$ regime (blue) is *k'* (*equation S7*). The concentration of acetate in the 40 equivalent experiment exhibits scatter due to the fact that DMA is nearly saturated at this concentration. The lower right is a plot of $1/k_{obs}$ vs. $[OAc]/[O]_2$ for the low $[O_2]$ regime for all three acetate concentrations.

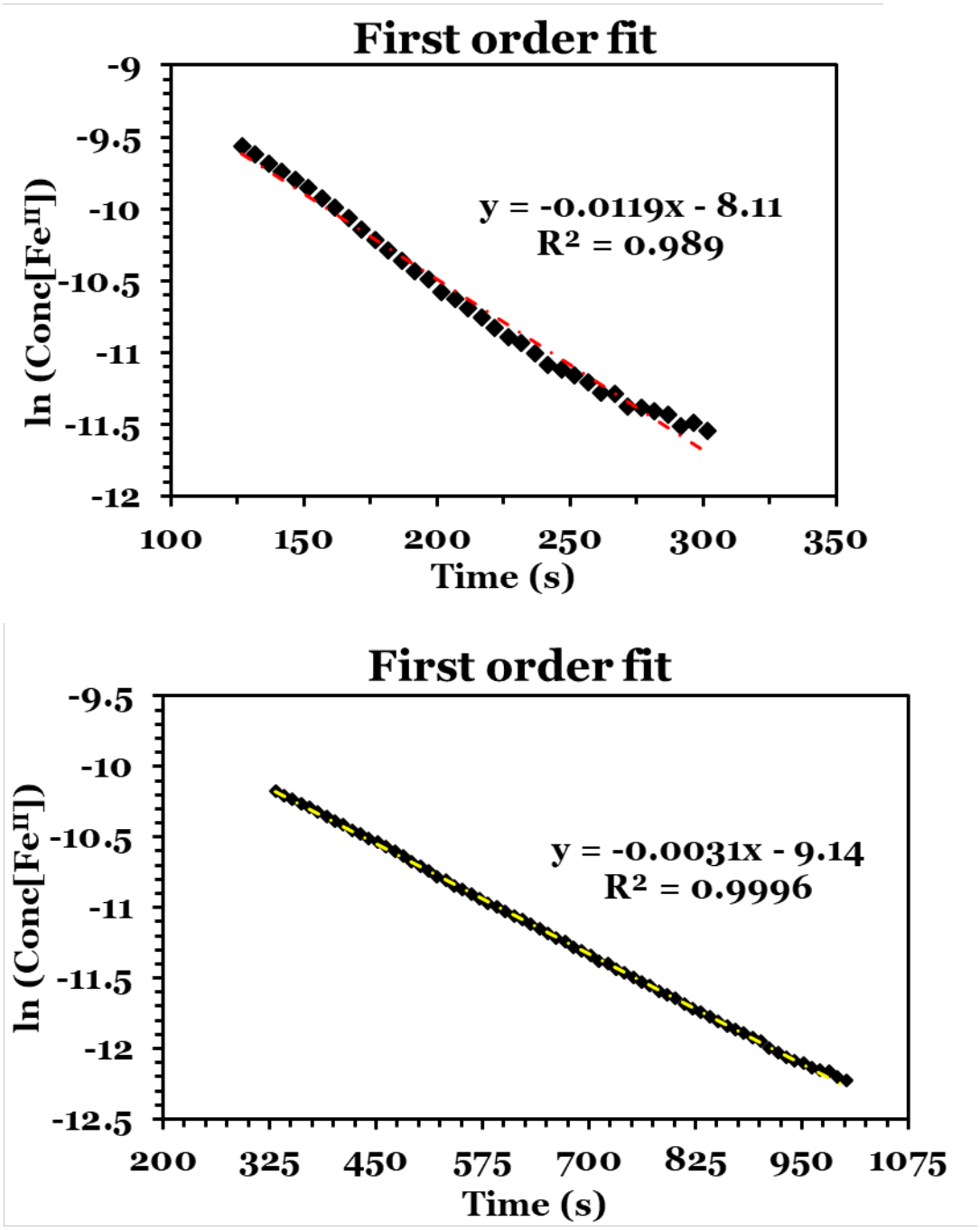

Figure S11. Representative first order plots for 0.1 mM $\mathbf{1}^{Cl}$ + O_2 (top) and 0.1 mM $\mathbf{1}^{NO_2}$ + O_2 (bottom) in DMA at 20 °C. Data was plotted out to three half-lives of the reaction.

Table S3. Data for Eyring plot for reaction between O_2 and 1^{NO_2} in DMA (plot shown to the right)

T (°C)	k_{obs}
-10	0.021
-10	0.022
-10	0.023
0	0.025
0	0.026
0	0.026
10	0.031
10	0.029
10	0.034
15	0.019
15	0.031
15	0.027
20	0.018
20	0.025
20	0.014
20	0.023
25	0.022
25	0.022
25	0.020
25	0.024
30	0.023
30	0.023
30	0.024
30	0.023
35	0.024
35	0.024
35	0.014
40	0.023
40	0.021
40	0.018
45	0.025
50	0.027
55	0.027
60	0.023
70	0.021
average	0.023±0.004

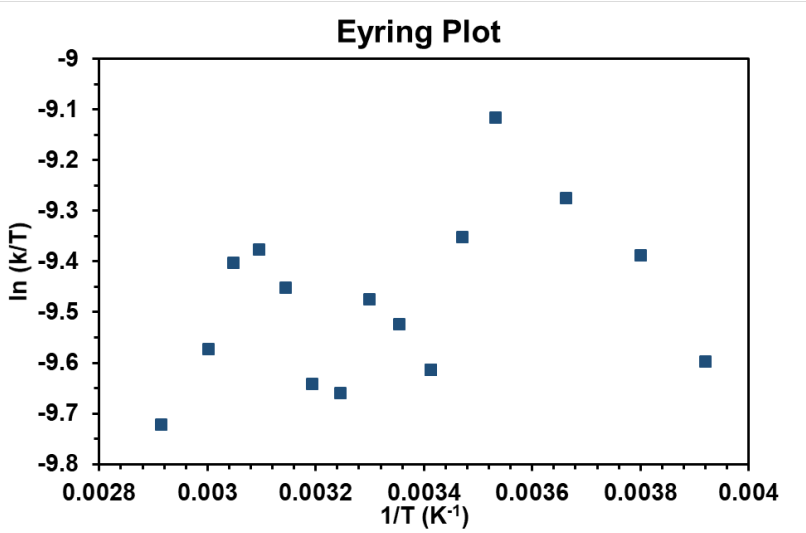

Kinetic Methods and Mass Transport Analysis for O_2 Diffusion

Sample preparation: All samples for kinetic experiments were prepared using dry DMA solvent that was passed through a celite plug to remove sieve dust in a glovebox under nitrogen atmosphere. Solutions of metal complex were used within 36 hours of preparation. Concentration of metal complex for experiments were 0.1 mM unless stated otherwise.

Measurements: For each trial, 3 ml of the sample was transferred to a Schlenk cuvette (Figure S12) adapted with a gas bulb, valves, and a side arm (Figure S12). The cell was closed and removed from the glovebox and connected to a Schlenk line. The Schlenk line was purged with argon and evacuated thrice. The side arm and gas bulb of the cuvette were evacuated and purged with argon thrice. The solution in the cuvette was cooled in an ice bath and then evacuated while stirring. The solution was degassed to a constant pressure of 125 mTorr. The cuvette was then isolated from the vacuum and the gas bulb was evacuated again. A known pressure of O_2 was added to the bulb using an oxygen tank and mercury manometer. Unless stated otherwise, the pressure was 1 atm. The bulb was then isolated from the Schlenk line and the cuvette was transferred to an 8154 Agilent spectrophotometer equipped with a Unisoku cryostat. The required temperature was set on the cryostat and the cuvette was allowed to equilibrate for 10 minutes. Data collection was initiated prior to exposing the DMA solution of iron complex to the O_2 The reaction was monitored by UV-Vis spectroscopy for 1000 – 1500 seconds which provided an adequate time period for the reaction to proceed three half-lives and the absorbance traces reached a plateau. The same stirrer speed was used for all experiments. The analysis of data was performed by traditional linear fits using Excel.

Transport of O_2 from headspace to DMA solution: After the initial exposure of the DMA solution to the O_2, a lag time was observed before changes appeared in the spectrum. This time period is caused by the process of O_2 dissolving in the solution and necessitates a mass transfer analysis. Such a mass transfer analysis of O_2 transport from the gas bulb to the solution revealed the delivery rate of O_2, the concentration profiles of O_2 in the gas and liquid phases, and time taken for the solution to reach pseudo-first order conditions (O_2 concentration ≥ 10·[$FeL^R(OAc)$]) . This analysis was performed using Euler's method for numerical integration and was executed on MATLAB with the appropriate temporal and spatial step sizes to satisfy the convergence criteria. The details regarding the mass transfer analysis are given below.

Mass Transfer Analysis for O_2 diffusion: The Schlenk cuvette was modeled as a vertical cylinder with a 1 cm x 1 cm x 3 cm cuvette at the bottom, which contains the solution (Figure S12). The gas bulb was treated as the top part of the cylinder having a diameter of 1 cm and height 14.9 cm so that the volume of this hypothetical cylinder would equal that of the gas bulb (11.7 cm^3). Similarly, the headspace above the cuvette was modeled as a continuing cylinder of diameter 1 cm and height 8.1 cm to accurately represent the geometry and volume of the headspace (3.9 ml).
The diffusion of O_2 through the gas phase was modeled using Fick's laws of diffusion and the dissolution equilibrium was calculated using Henry's Law. The solution was considered to be perfectly mixed, so there was no boundary layer or concentration gradient in solution. In addition, only diffusion in the z-direction was considered.

The transfer of O_2 can be divided into three parts as shown in Figure S12: the self-diffusion of O_2 through the gas bulb (***A***), the diffusion of O_2 through the headspace (***B***), and the dissolution of O_2 (***C***). Each of these three parts is labeled as follows…

$$Gas\ bulb = \boldsymbol{A}$$
$$Headspace = \boldsymbol{B}$$
$$Solution = \boldsymbol{C}$$

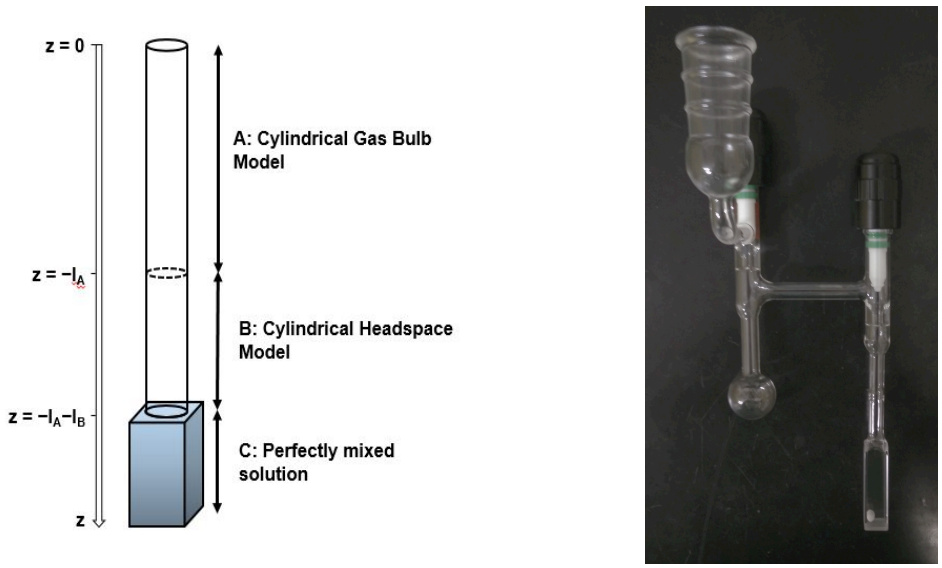

Figure S12. Model for gas diffusion (left). Image of the actual Schlenk cuvette (right).

The diffusion of O_2 through ***A*** is given by Fick's second law and is written as,

$$\frac{\partial P_{O_2}(t,z)}{\partial t} = D_{O_2A}\frac{\partial^2 P_{O_2}(t,z)}{\partial z^2} \qquad \textit{equation S20}$$

Where, P_{O2} is the partial pressure of O_2 at any position z in ***A*** at any given time *t*; D_{O2A} is the diffusion coefficient for O_2 through ***A***. Since the gas bulb is filled with only O_2, D_{O2A} is the same as D_{O2O2}, the self-diffusion coefficient for O_2 and can be calculated by the following equation.[3]

$$D_{O_2O_2} = \frac{2T^{\frac{3}{2}}}{3\pi^{\frac{3}{2}}\sigma_{O_2}{}^2 P}\left(\frac{k_B{}^3 N_{Av}}{MW_{O_2}}\right)^{1/2} \qquad \textit{equation S21}$$

Where, T is the temperature in Kelvin, k_B is the Boltzmann constant in ergs/K, N_{Av} is the Avagadro's constant, MW_{O2} is the molecular weight of O_2 in g/mol, *P* is the pressure of the system in g/(cm s^2) and σ_{O2} is the Lennard-Jones diameter for O_2 in cm.
Similarly, the diffusion of O_2 through ***B*** is given by,

$$\frac{\partial P_{O_2}(t,z)}{\partial t} = D_{O_2B}\frac{\partial^2 P_{O_2}(t,z)}{\partial z^2} \qquad \textit{equation S22}$$

Where, P_{O2} is the partial pressure of O_2 at any position z in ***B*** at any given time *t*; D_{O2B} is the diffusion coefficient for O_2 through ***B***. Since ***B*** is initially nitrogen, D_{O2B} is D_{O2N2} can be calculated using the Hirschfelder equation[3] shown below.

$$D_{O_2N_2} = \frac{0.001858T^{\frac{3}{2}}\left[\frac{1}{MW_{O_2}}+\frac{1}{MW_{N_2}}\right]^{\frac{1}{2}}}{P\sigma^2_{O_2N_2}\boldsymbol{\Omega}_D} \qquad \textit{equation S23}$$

Where, T is the temperature in K, MW_{O2} is the molecular weight of O_2 in g/mol, MW_{N2} is the molecular weight of N_2 in g/mol, *P* is the system pressure in atm, σ_{AB} is the collision diameter, a Lennard–Jones parameter, in Å, and Ω_D is the collision integral for molecular diffusion. However as time passes, the head space is filled with a pressure gradient of O_2 and so D_{O2B} then becomes D_{O2O2}, the self-diffusion coefficient which can be calculated by equation S21 above. The Lennard-Jones parameters for O_2 and N_2 were obtained from Appendix K in Welty, Wicks, Wilson and Rorrer.[3] Since the solution, ***C*** is considered to be perfectly mixed, there is no concentration gradient in ***C*** at any given time. The mole fraction of oxygen in

C was calculated using Henry's law and the Henry's constant for O_2 in DMA was found to be 2074 atm based on the findings of Yamamoto et al.[4]

$$P_{O_2}(t) = xH \qquad \textit{equation S24}$$

Where, P_{O2} is the partial pressure of O_2 at the surface of the solution, x is the mole fraction of O_2 in solution and H is the henry's constant (2074 atm). The concentration of O_2 in solution can be calculated at any given time as follows.

$$n_{total} \approx n_{solvent} + n_{\mathrm{FeL}^{R}(\mathrm{OAc})} \qquad \textit{equation S25}$$

$$n_{O_2} = x * n_{total} \qquad \textit{equation S26}$$

$$[O_2] = \frac{n_{O_2}}{V} \qquad \textit{equation S27}$$

Where V is the volume of the solution and is taken to be 3 ml or 0.003 L. In addition to these equations, the flux N_{O2} at any position at any given time can be expressed as the following equations.
By Fick's first law of diffusion,

$$N_{O_2}^{P}(z,t) = -D_{O_2 i}\frac{\partial P_{O_2}(z,t)}{\partial z} = \frac{\partial P_{O_2}(z,t)}{\partial t}\frac{1}{Ac} \qquad \textit{equation S28}$$

Where, $N_{O2}{}^{P}$ is the pressure flux at any point z at any time t, D_{O2i} is the diffusion coefficient for O_2 through medium i (i = ***A***, ***B***, or ***C***), P_{O2} is the partial pressure of O_2 at any point z at any time t and Ac is the cross-sectional area through which the mass transfer occurs. The pressure fluxes can be converted to concentration fluxes by utilizing the ideal gas law as necessary.

The partial differential equations above were solved with the following initial and boundary conditions shown below using finite difference approximations and numerical integration with Euler's method. The numerical integration was performed on a 2-dimensional grid comprising of spatial nodes along one direction and temporal nodes along the other. The gas bulb, i.e. region ***A*** was divided into 10 nodes starting at z = 0 to z = -l_A where l_A is the height of the cylindrical model for the gas bulb.

$$n_A = 10; dz_A = \frac{-l_A}{n_A} = -1.49\ cm \qquad \textit{equation S29}$$

The headspace, i.e. region ***B*** was divided into 10 nodes starting at z = -l_A to z = -l_B where l_B is the height of the cylindrical model for the headspace.

$$n_B = 10; dz_B = \frac{-l_B-(-l_A)}{n_A} = -0.81\ cm \qquad \textit{equation S30}$$

The solution, region ***C***, is treated as a single node lying at z = -l_A-l_B. This set of nodes constitutes the spatial dimension of the grid. The temporal nodes were set starting from t = 0 seconds to t = 300 seconds. The time step dt was set as 0.0001 seconds in order to satisfy the convergence criteria for Euler's method.

$$n_t = 3{,}000{,}000; dt = 0.0001\ s \qquad \textit{equation S31}$$

Thus a grid containing 22 spatial nodes and 3,000,000 temporal nodes was obtained. The following sequence of calculations must be performed at each temporal node in order to progress through the grid and obtain the pressure and concentration profiles of O_2 at any given time.

At the top of the gas bulb at any time t, z = 0 and n_A = 1. The partial derivatives in equation 1 can be approximated using first and second order finite differences as shown below.

$$\frac{\partial P_{O_2}(t,z)}{\partial t} = \frac{\left(P_{O_2}(t,n_A) - P_{O_2}(t-1,n_A)\right)}{dt} \qquad \textit{equation S32}$$

$$\frac{\partial^2 P_{O_2}(t,z)}{\partial z^2} = \frac{P_{O_2}(t-1,n_A+2) - 2P_{O_2}(t-1,n_A+1) + P_{O_2}(t-1,n_A)}{dz_A{}^2} \quad \textit{equation S33}$$

Substituting these in equation S20 and solving for $P_{O2}(t, n_A)$ we get,

$$P_{O_2}(t,n_A) = \frac{D_{O_2A}dt}{dz_A^2}\left(P_{O_2}(t-1,n_A+2) - 2P_{O_2}(t-1,n_A+1) + P_{O_2}(t-1,n_A)\right) + P_{O_2}(t-1,n_A)$$

For all other interior spatial nodes in ***A***, a similar expression can be obtained using equation S20. However for interior nodes, n_A = 2 to 10. So the following calculation must be performed for each spatial node n_A at each time step. The following first order finite difference approximations were used.

$$\frac{\partial P_{O_2}(t,z)}{\partial t} = \frac{\left(P_{O_2}(t,n_A) - P_{O_2}(t-1,n_A)\right)}{dt} \quad \textit{equation S34}$$

$$\frac{\partial^2 P_{O_2}(t,z)}{\partial z^2} = \frac{P_{O_2}(t-1,n_A+1) - 2P_{O_2}(t-1,n_A) + P_{O_2}(t-1,n_A-1)}{dz_A{}^2} \quad \textit{equation S35}$$

Substituting these in equation S20 and solving for $P_{O2}(t, n_A)$ we get,

$$P_{O_2}(t,n_A) = \frac{D_{O_2A}dt}{dz_A^2}\left(P_{O_2}(t-1,n_A+1) - 2P_{O_2}(t-1,n_A) + P_{O_2}(t-1,n_A-1)\right) + P_{O_2}(t-1,n_A) \quad \textit{equation S36}$$

At the bottom of region ***A***, n_A = 11 and $z = -l_A$. This node represents the interface between ***A*** and ***B*** and so the partial pressure of O_2 at n_A = 11 is the same as the partial pressure of O_2 at n_B = 1. Using the condition for equality of fluxes, i.e. the flux of O_2 from region ***A*** must equal the flux of O_2 into region ***B***, the following expression can be obtained.

$$N_{O_2}^A(z,t) = N_{O_2}^B(z,t) \quad \textit{equation S36}$$

However, we know that

$$N_{O_2}^A(z,t) = -D_{O_2A}\frac{\partial P_{O_2}(z,t)}{\partial z} \quad \textit{equation S37}$$

Similarly,

$$N_{O_2}^B(z,t) = \frac{\partial P_{O_2}(z,t)}{\partial t}\frac{1}{Ac} \quad \textit{equation S38}$$

Therefore

$$-D_{O_2A}\frac{\partial P_{O_2}(z,t)}{\partial z} = \frac{\partial P_{O_2}(z,t)}{\partial t}\frac{1}{Ac} \quad \textit{equation S39}$$

Using the following first and second order finite difference approximations,

$$\frac{\partial P_{O_2}(t,z)}{\partial t} = \frac{\left(P_{O_2}(t,n_B) - P_{O_2}(t-1,n_B)\right)}{dt} \quad \textit{equation S40}$$

$$\frac{\partial P_{O_2}(z,t)}{\partial z} = \frac{(3P_{O_2}(t-1,n_A) - 4P_{O_2}(t-1,n_A-1) + P_{O_2}(t-1,n_A-2))}{2dz_A} \quad \textit{equation S41}$$

Equation S39 can then be solved for $P_{O2}(t,n_B)$

$$P_{O_2}(t,n_B) = P_{O_2}(t-1,n_B) - \frac{AcD_{O_2A}dt}{2dz_A}(3P_{O_2}(t-1,n_A) - 4P_{O_2}(t-1,n_A-1) + P_{O_2}(t-1,n_A-2))$$

equation S42

$$P_{O_2}(t,n_A) = P_{O_2}(t,n_B)$$

Here Ac is the cross-sectional area for the interface between ***A*** and ***B*** in cm². Now all the values for P_{O_2} in region ***A*** and the P_{O_2} at $n_B = 1$ at time t have been calculated. The interior nodes for ***B*** are calculated in a manner similar to the interior nodes of ***A***. The equation for $P_{O_2}(t, n_B)$ is given below,

$$P_{O_2}(t, n_B) = \frac{D_{O_2B}dt}{dz_B^2}\left(P_{O_2}(t-1, n_B+1) - 2P_{O_2}(t-1, n_B) + P_{O_2}(t-1, n_B-1)\right) + P_{O_2}(t-1, n_B) \quad \textit{equation S43}$$

At the final node in ***B***, $n_B = 11$, the partial pressure of O_2 is in equilibrium with the solution. This equilibrium is expressed as Henry's law. In addition, the gas-solution interface between ***B*** and ***C*** is similar to gas-gas interface between ***A*** and ***B*** and so applying the condition for equality of fluxes, we get,

$$N_{O_2}^B(z, t) = N_{O_2}^C(z, t) \quad \textit{equation S44}$$

Therefore,

$$-D_{O_2B}\frac{\partial P_{O_2}(z,t)}{\partial z} = \frac{\partial P_{O_2}(z,t)}{\partial t}\frac{1}{Ac} \quad \textit{equation S45}$$

However, since ***C*** is a solution, it is more convenient to convert the pressure flux in ***C*** to a molar flux. This can be achieved using the ideal gas law. This then yields,

$$\left(-D_{O_2B}\frac{\partial P_{O_2}(z,t)}{\partial z}\right)\left(\frac{V}{RT}\right) = \frac{\partial n_{O_2}(z,t)}{\partial t}\frac{1}{Ac} \quad \textit{equation S46}$$

Where, V is the volume of the solution and is taken to be 3 ml or 0.003 L, R is the gas constant in consistent units and T is the temperature in K. Ac is the cross-sectional area of the interface between ***B*** and ***C***.

$$\frac{\partial n_{O_2}(t,z)}{\partial t} = \frac{\left(n_{O_2}(t, n_C) - n_{O_2}(t-1, n_C)\right)}{dt} \quad \textit{equation S47}$$

$$\frac{\partial P_{O_2}(z,t)}{\partial z} = \frac{(3P_{O_2}(t-1, n_B) - 4P_{O_2}(t-1, n_B-1) + P_{O_2}(t-1, n_B-2))}{2dz_B} \quad \textit{equation S48}$$

Equation S46 then becomes,

$$n_{O_2}(t, n_C) = n_{O_2}(t-1, n_C) - \frac{AcD_{O_2B}dtV}{2dz_BRT}(3P_{O_2}(t-1, n_B) - 4P_{O_2}(t-1, n_B-1) + P_{O_2}(t-1, n_B-2))$$

equation S49

The mole fraction of O_2 then becomes,

$$x = \frac{n_{O_2}}{n_{total}};\ n_{total} \approx n_{solvent} + n_{\mathrm{FeL}^R(OAc)} \quad \textit{equation S50}$$

Then using Henry's law,

$$P_{O_2}(t, n_B + 1) = xH \quad \textit{equation S51}$$

The concentration of O_2 in the solution can also be calculated using n_{O2}. Thus the concentration and partial pressure profile at all spatial nodes can be calculated for a given temporal node *t*. This was achieved using MATLAB and the results are shown below in Figure S13.

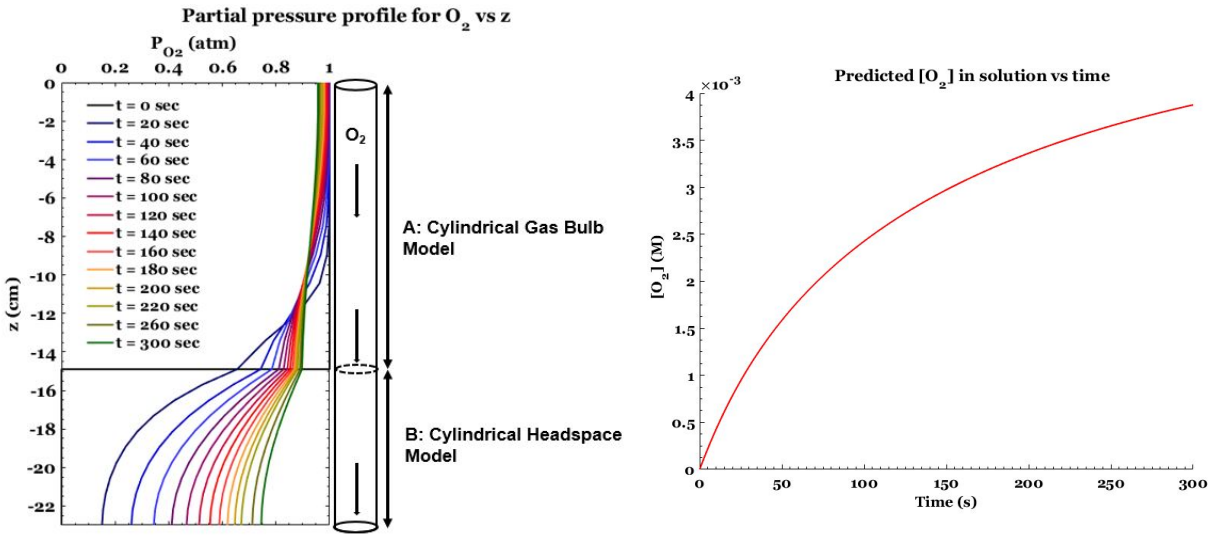

Figure S13. Pressure profiles for O_2 in the gas bulb and headspace of the Schlenk cuvette at different times ranging from 0 seconds to 300 seconds during a kinetic run (left). Concentration of O_2 dissolved in solution as a function of time (right) as predicted by the diffusion model. The calculation was performed on MATLAB using the O2_diffsuion script. Starting conditions: Headspace pressure prior to O_2 addition = 125 mTorr N_2; pressure of O_2 in the gas bulb = 1 atm.

Application of Mass transport analysis to kinetic analysis: While the mass transfer model enables us to understand the process by which oxygen gets added to the solution, it does not directly enable us to analyze each kinetic run. However using the knowledge from the model, it is possible to accurately analyze the data from each kinetic run specifically in the pseudo first order region. When a kinetic run is started, the O_2 diffuses across the headspace and begins to dissolve in the solution. This is the early part of the absorbance trace where essentially no reaction is seen. Soon the reaction becomes observable but the concentrations of O_2 is roughly equal to the concentration of $[FeL^R(OAc)]^{2-}$. Furthermore, the rate of dissolution of O_2 in DMA is can be expected to be larger than the rate of reaction of O_2 with the iron complex and so there is a net accumulation of O_2 in solution at the early stages. As the solution approaches saturation, the rate of dissolution decreases and eventually becomes lower than the rate of the reaction. As a consequence of this complicated interplay between the rate of dissolution of O_2 and reaction, the initial changes in the absorbance traces cannot be taken to be representative of the pseudo-first order region of the reaction. For each kinetic run, the observed rate of reaction at each time point can be calculated from the concentration of Fe^{II} species at that time which is in turn calculated from the absorbance trace at the appropriate wavelength.

$$rate = \frac{[Fe^{II}]_{t2} - [Fe^{II}]_{t1}}{t2 - t1} \qquad \textit{equation S52}$$

A plot of this rate vs time yields Figure S14. From this Figure it can be seen that there is an initial increase in the rate of the reaction during the same time period that would be expected for O_2 dissolution. This would make sense because the resulting net accumulation of O_2 in solution would result in an increase in the rate of the reaction. However as the solution reaches a concentration of O_2 much larger than that of the iron compound, the rate becomes dependent only on the iron and so from this point on we can begin a first order kinetic analysis. All kinetic runs show this trend where there is an initial increase in the rate that is then followed by a transition to the characteristic exponential decay for pseudo-first order

conditions. Using this information, all kinetic runs were analyzed from the time when the rate of the reaction reached its maximum.

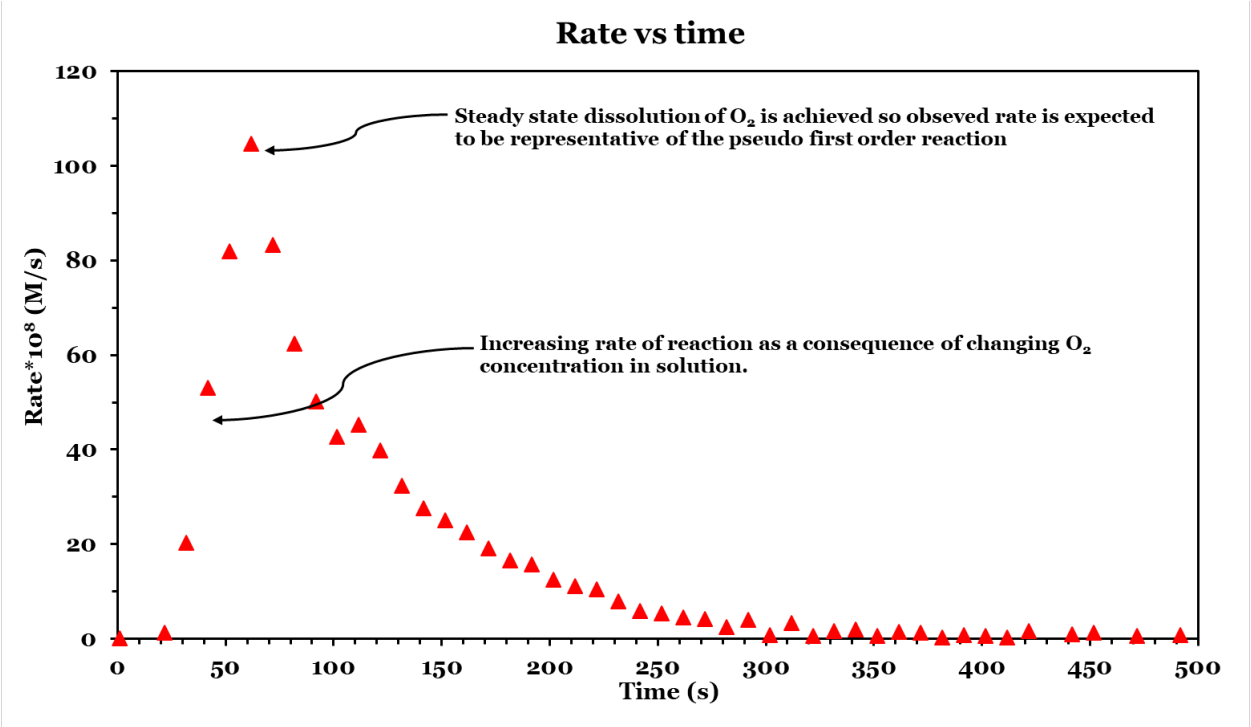

Figure S14. The rate of reaction approximated at each step using finite differences plotted as a function of time. For example, this data was used to construct the plots in Figure S8.

References

1. Ray, M.; Golombek, A. P.; Hendrich, M. P.; Yap, G. P. A.; Liable-Sands, L. M.; Rheingold, A. L.; Borovik, A. S. Structure and magnetic properties of trigonal bipyramidal iron nitrosyl complexes. *Inorg. Chem.* **1999**, *38*, 3110-3115.
2. Hansch, C.; Leo, A.; Taft, R. W. A Survey of Hammett Substituent Constants and Resonance and Field Parameters *Chem. Rev.* **1991**, *91*, 165-195.
3. Welty, J. R.; Wicks, C.E.; Wilson, R. E.; Rorrer, G.L. *Fundamentals of Momentum, Heat, and Mass Transfer*; John Wiley and Sons, Inc.: United States, 2008.
4. Sato, T.; Hamada, Y.; Sumikawa, M.; Araki, S.; Yamamoto, H., Solubility of Oxygen in Organic Solvents and Calculation of the Hansen Solubility Parameters of Oxygen. *Ind. Eng. Chem. Res.* **2014,** *53* (49), 19331-19337.